Preprint DAMTP 96-77, PUPT-1640
e-Print Archive: hep-ph/9608350

arXiv:hep-ph/9608350v3 14 May 1997

Classical Field Dynamics of the Electroweak Phase Transition

Guy D. Moore[1]

Princeton University
Joseph Henry Laboratories, PO Box 708
Princeton, NJ 08544, USA

Neil Turok [2]

DAMTP, Silver Street
Cambridge, CB3 9EW, UK

Abstract

We investigate the thermodynamics and dynamics of the electroweak phase transition by modelling the infrared physics with classical Yang-Mills Higgs theory. We discuss the accuracy of this approach and conclude that, for quantities whose determination is dominated by the infrared, the classical method should be correct up to parametrically suppressed (ie $O(\alpha)$) corrections. For a Higgs self-coupling which at tree level corresponds to $m_H \simeq 50$GeV, we determine the jump in the order parameter to be $\delta\phi = 1.5gT$, the surface tension to be $\sigma = 0.07g^4T^3$, and the friction coefficient on the moving bubble wall due to infrared bosons to be $\eta \equiv P/v_w = 0.03 \pm .004g^6T^4$. We also investigate the response of Chern-Simons number to a spatially uniform chemical potential and find that it falls off a short distance inside the bubble wall, both in equilibrium and below the equilibrium temperature.

PACS numbers: 03.50.Kk, 11.10.Wx, 11.15.Ha, 11.15.Kc

Keywords: classical field theory, electroweak phase transition, lattice gauge theory, baryon number, sphaleron, bubble wall velocity

[1]e-mail: guymoore@puhep1.princeton.edu
[2]e-mail: N.G.Turok@damtp.cam.ac.uk

1 Introduction

Since Sakharov proposed that the universe's baryon number could have been generated dynamically early in the Big Bang [1], many different particle physics scenarios have been proposed to realize this mechanism. One of the most interesting is based on the observation made 20 years ago by t'Hooft that baryon number is violated already in the minimal standard model [2]; and by the later realization that the violation is very efficient at temperatures above the electroweak phase transition temperature, where the Higgs condensate is absent [3, 4]. It was subsequently shown that electroweak baryogenesis could actually occur in minimal extensions of the standard model involving one or more additional Higgs doublets, and that the resulting asymmetry was naturally of the order of magnitude required in cosmology [5], [6]. Other, potentially more efficient baryogenesis mechanisms were proposed [7, 8], both in these theories and in other extensions of the standard model. What is most exciting about these scenarios is that they link the origin of matter in the universe to physics beyond the standard model that could be probed by the next generation of Higgs-seeking accelerators, and other experiments looking for novel sources of C and CP violation.

Because of these developments there has been quite intense interest in the electroweak phase transition. But the quest to understand baryogenesis at the electroweak scale has been bedeviled by difficulties. It is now believed that we know what basic issues are involved. As temperature drops, the Higgs field develops a condensate abruptly in a first order phase transition. This proceeds by the nucleation and subsequent growth of bubbles of the low temperature, broken symmetry phase. Outside the bubbles, baryon number is violated, but inside it is conserved. The plasma departs from equilibrium on and very near the boundaries of these bubbles, and if there is some CP violation, for instance in the Higgs sector, then all necessary conditions for the creation of a baryon number excess exist; and it would be preserved to this day because the rate of baryon number violation is very low inside the bubbles, if the phase transition is suitably strong. It is also strongly believed that the communication of the C and CP violating physics to the infrared gauge-Higgs fields, which are responsible for the baryon number violation, should be conducted by the fermions, and that the transport of the fermions in the presence of the wall may be relevant. But turning this understanding into predictions requires an accurate description of the dynamics of the phase transition, which has so far been poorly developed. The dynamics, in turn, cannot be well understood until the thermodynamics are under control; and all aspects require a complete knowledge of the underlying electroweak physics, which of course is still lacking.

In the coming years we will hopefully learn the required information about electroweak physics, for instance the exact nature of the Higgs mechanism, the existence or absence of low energy supersymmetry, and details of any non-CKM CP violation. But our ignorance of these details does not prevent work on the thermodynamics and dynamics of the electroweak phase transition from proceeding. The tools developed to investigate the simplest case, the minimal standard model, should be straightforward to extend to more complicated models; in fact the extension may often be analytically

tractable, as seems to be the case generically for the thermodynamics [9, 10].

One tool which has proven less useful than hoped is perturbation theory. While one loop perturbation theory can determine the phase transition temperature with $O(\alpha)$ accuracy [11], it is less reliable for the details of the phase transition, such as the jump in the order parameter, the latent heat, the surface tension, and so forth. This became clear when Arnold and Espinosa computed the effective potential to two loops [12, 13]. At one loop a term of form $-g^3\phi^3 T/\pi$ arises which generates a Higgs vev squared of $\phi^2 \sim g^6 T^2/\lambda^2\pi^2$; and at two loops a new term of form $-g^4\phi^2 T^2 \ln(\phi/T)/\pi^2$ arises, which alone would generate $\phi^2 \sim g^4 T^2/\lambda\pi^2$. As far as the strength of the phase transition is concerned, perturbation theory is at best an expansion in λ/g^2, or $(m_H/m_W)^2$.

Because λ receives large radiative corrections, it is difficult to make the ratio λ/g^2 very small; we also know that, if the minimal standard model is correct, the ratio cannot be small, because direct searches for the Higgs boson have ruled it out below a mass of 60GeV. It therefore seems reasonable to take $\lambda \sim g^2$ parametrically. This is also natural from the point of view of unit analysis, if we allow $\hbar$ to be dimensionful. To do otherwise would require a rearrangement of perturbation theory away from the usual loopwise expansion, which can be understood in the vacuum theory as an expansion in powers of $\hbar$. We see from the above discussion, though, that at the phase transition temperature, for quantities such as the jump in the order parameter, the perturbation series is not an expansion in $\hbar$, which helps to explain its poor convergence.

Farakos et. al. have elucidated the reason for this, by showing how the infrared thermodynamics of the minimal standard model at finite temperature is very well described by a "dimensionally reduced" 3 dimensional field theory [14]. this analysis has allowed an efficient nonperturbative investigation of the phase transition which is now bearing fruit [15, 9, 16].

An at first sight unrelated development is the idea that the rate of anomalous baryon number violation in the high temperature phase of the classical theory is computable numerically, and that the rate in the classical theory should be the same, up to $O(\alpha)$ corrections, as the rate in the quantum theory [17, 18, 19]. This has allowed the first quantitative measurement of a dynamical, infrared property of finite temperature Yang-Mills Higgs theory above the phase transition temperature. The validity of this idea is fortified by the observation that the thermodynamics of the classical theory coincides with the thermodynamics of the quantum theory in the approximation of dimensional reduction [20].

In fact we believe that the success of the dimensional reduction technique, and the nonperturbative nature of the infrared quantum theory, arise precisely because the infrared bosonic modes attain large occupation numbers which cause the theory to mimic a classical theory. We will argue in Section 2 that this mimicry extends to the dynamics, so that all infrared dominated dynamical properties of the theory which possess cutoff independent limits in the classical theory will take the same value, up to $O(\alpha)$ corrections, in the quantum theory. We then review an evolution algorithm for the lattice cut off, classical field theory in Section 3. Since the classical theory has the same thermodynamics as the quantum theory in the dimensional

reduction approximation, this evolution algorithm is also a microcanonical Monte-Carlo algorithm for the dimensionally reduced theory; so we develop and apply the tools for using it to investigate the thermodynamics of the phase transition in Section 4. Then we turn to dynamics; in Section 5 we use the classical technique to compute the contribution of infrared bosons to the friction felt by a moving bubble wall as it sweeps through the plasma, in a near equilibrium approximation. In Section 6 we investigate baryon number violation in the presence of an out of equilibrium bubble wall. Section 7 concludes. There are also two appendicies. Appendix A presents the tools for the numerical study of Chern-Simons number (N_{CS}) motion, and investigates baryon number violation in each phase; in particular it presents evidence that the observed rate of baryon number violation in the broken phase arises from ultraviolet lattice artefacts. Appendix B presents the details of how to extract the surface tension of the bubble wall.

We make no serious attempt to extrapolate to the continuum limit either for the thermodynamical or dynamical properties, so the results presented here should be considered rough and preliminary; the emphasis is on development of techniques.

2 Discussion of the classical approximation

As discussed in the introduction, we will investigate the use of classical Yang-Mills Higgs theory as a surrogate for the Standard Model. In important respects the classical theory does not resemble the quantum theory at all (for instance, it has an infinite, or cutoff dependent, heat capacity); it should only be used for those dynamical and thermodynamical properties which are dominated by infrared physics, where it should give results which reproduce the parametrically leading term in the full quantum theory. Hence, for instance, the classical theory has been used to investigate baryon number violation in the symmetric electroweak phase, a phenomenon thought to be infrared dominated [17, 18, 19, 20, 21, 22, 23]. It has also been used, in a slight disguise, to investigate the thermodynamics of the phase transition.

To see the latter point, consider the dimensional reduction program of Farakos et al [24, 15, 9, 16], a systematic, semiperturbative approach to determining the strength and other thermodynamic properties of the phase transition. Their idea is the following. All thermodynamic properties can be derived in the Matusbara formulism, ie by considering a Euclidian path integral in which time runs from 0 to $\beta = 1/T$ with periodic boundary conditions for bosons and antiperiodic boundary conditions for fermions. To compute the thermal expectation value of an operator $\mathcal{O}$, we find

$$\langle \mathcal{O} \rangle = \frac{\int \mathcal{D}\Phi \mathcal{D}A^\mu \mathcal{O} \exp(-S)}{\int \mathcal{D}\Phi \mathcal{D}A^\mu \exp(-S)}\,, \tag{1}$$

$$S \equiv \int_0^\beta dx_0 \int d^3x (\mathcal{L} + \mathcal{L}_{\rm ct})\,,$$

$$\mathcal{L} \equiv \frac{1}{4g_4^2} F^a_{\mu\nu} F^a_{\mu\nu} + (D_\mu \Phi)^\dagger D_\mu \Phi + m_{H4}^2 \Phi^\dagger \Phi + \lambda_4 (\Phi^\dagger \Phi)^2\,. \tag{2}$$

The subscript 4 means that these values depend on renormalization point exactly as they do in the 4 dimensional vacuum theory, as do the wave functions; the theory also requires counterterms represented by $\mathcal{L}_{\rm ct}$. (For simplicity we have not written terms involving fermions, but they should be present.) By Fourier transforming the time direction, one obtains a 3 dimensional theory in which the Fourier components with nonzero Matsubara frequency appear as a Kaluza-Klein tower of massive modes. Following [25], they construct an infrared effective theory of the zero frequency mode, integrating out the massive modes by computing a set of correlators in each theory and matching them in the infrared. Provided that the operator $\mathcal{O}$ consists of spatially extended, equal time combinations of bosonic operators, its expectation value is then well approximated by

$$\begin{aligned} \langle \mathcal{O} \rangle &= \frac{\int \mathcal{D}\Phi \mathcal{D}A^\mu \mathcal{O} \exp(-\beta H)}{\int \mathcal{D}\Phi \mathcal{D}A^\mu \exp(-\beta H)} \,, & (3) \\ \beta H &\equiv \beta \int d^3x \frac{1}{4g^2} F_{ij}^a F_{ij}^a + (D_i\Phi)^\dagger D_i \Phi + \frac{1}{2} D_i A_0^a D_i A_0^a + \frac{g^2}{4} A_0^2 \Phi^\dagger \Phi + \\ & \frac{m_{D0}^2}{2} A_0^2 + m_{H0}^2 \Phi^\dagger \Phi + \lambda (\Phi^\dagger \Phi)^2 \,. & (4) \end{aligned}$$

Here the wave functions and couplings do not renormalize but have their values fixed (at a given temperature) by the matching process. (We have dropped an extremely small A_0^4 term and a slight correction to the coefficient in the $A_0^2 \Phi^\dagger \Phi$ term, as in [15].) The mass terms, on the other hand, do depend on the renormalization procedure, as indicated by the subscript 0, meaning the bare values. They are related to the renormalized values, determined in the perturbative matching procedure, by

$$m_D^2(\mu) = m_{D0}^2 + \delta m_D^2(\mu) \,, \qquad (5)$$

and similarly for m_H^2. In regulations where linear divergences do not vanish, such as lattice regulations, the counterterm is substantial and positive, so the bare mass squared may need to be small or negative.

We have deliberately used different notation than Farakos et. al. to emphasize that the path integral is over an action which looks like H/T, with H "almost" the Hamiltonian of the classical theory.

To investigate the relationship between the dimensionally reduced theory above and the thermodynamics of the classical bosonic theory, we follow a line of reasoning developed in [20]. In the classical theory, thermodynamics are described by the partition function

$$\begin{aligned} Z &= \int \mathcal{D}A_i^a \mathcal{D}E_i^a \mathcal{D}\Pi \mathcal{D}\Phi \delta \left((D_i E_i)^a + g^2 {\rm Re}\Pi \frac{i\tau^a}{2} \Phi \right) \exp(-\beta H) & (6) \\ H &= \frac{1}{g^2} \left(\frac{1}{4} F_{ij}^a F_{ij}^a + \frac{1}{2} E_i^a E_i^a \right) + \Pi^\dagger \Pi + (D_i \Phi)^\dagger D_i \Phi + & (7) \\ & m_{H0}^2 \Phi^\dagger \Phi + \lambda (\Phi^\dagger \Phi)^2 \,, \end{aligned}$$

where the delta function enforces Gauss' law. It can be written by introducing an

integration over a Lagrange multiplier A_0^a and adding to the Hamiltonian

$$iA_0^a \left(\frac{(D_i E_i)^a}{g} + g\mathrm{Re}\Pi \frac{i\tau^a}{2}\Phi \right) . \tag{8}$$

The measure for E_i^a and Π is now trivial and the integrals are Gaussian. Performing them, the partition function becomes

$$\begin{aligned} Z &= \int \mathcal{D}\Phi \mathcal{D}A_\mu \exp(-\beta H) & (9) \\ H &= \int d^3x \frac{1}{4g^2} F_{ij}^a F_{ij}^a + (D_i\Phi)^\dagger D_i\Phi + \frac{1}{2} D_i A_0^a D_i A_0^a + \frac{g^2}{4} A_0^2 \Phi^\dagger \Phi + \\ & \quad 0A_0^2 + m_{H0}^2 \Phi^\dagger\Phi + \lambda(\Phi^\dagger\Phi)^2 , & (10) \end{aligned}$$

identical to Eq. (4) except that m_{D0}^2 is forced to be zero. The actual Debye mass squared then equals the counterterm. In lattice regulation, the counterterm turns out to be [15]

$$\delta m_D^2 \simeq \frac{5g^2\Sigma T}{4\pi a} , \qquad \Sigma = 3.17591 , \tag{11}$$

which grows linearly with $1/a$. One choice is to set the lattice spacing a so that this is actually the correct Debye mass, but this is not essential. All that is really needed is that the screening be efficient enough that the influence of the A_0 field on the infrared physics should be perturbatively computable (which is the case for the physical value of m_D, and is true for the value in Eq. (11) for reasonable values of a). In this case we can use the results of [15] to relate the thermodynamics of the lattice system to the thermodynamics without the A_0 field, which in turn can be related to the thermodynamics with the A_0 field and the appropriate Debye mass. Except for the need for this correction, an investigation of the thermodynamics of the classical theory is equivalent to an investigation of the dimensionally reduced theory.

The preceding discussion suggests a profound connection between the thermodynamics of the classical theory and the nonperturbative infrared physics of the quantum theory. To explore whether the connection extends to real time properties, we will briefly investigate the real time perturbative expansion of each theory.

Let us start with classical field theory. For simplicity we shall take as usual the example of $\lambda\phi^4$ scalar field theory, and we assume some regularization, like lattice regularization, is present. The classical thermal ensemble is defined as:

$$\langle \mathcal{O} \rangle_\beta = \frac{\int \mathcal{D}\phi_i \mathcal{D}\pi_i \exp(-\beta H(\pi_i, \phi_i))\mathcal{O}}{\int \mathcal{D}\phi \mathcal{D}\pi \exp(-\beta H(\pi_i, \phi_i))} \tag{12}$$

where $\mathcal{O}$ is some quantity of interest. The classical field $\phi_i(\mathbf{x})$ and its momentum $\pi_i(\mathbf{x})$ are those at some particular initial time t_i: the measure is to be thought of as a measure on the space of initial conditions for the field. The Hamiltonian H is $H_0 + H_{int}$, with $H_0 = \int d^3x \frac{1}{2}(\pi_i^2 + \phi_i^2)$ and $H_{int} = \frac{1}{24}\int d^3x \lambda \phi_i^4$. Since both the measure and the Hamiltonian are time independent, the expectation value $\langle \mathcal{O} \rangle_\beta$ is independent of t_i. As far as $\mathcal{O}$ is concerned, it may be any function of the classical

field and momentum, evaluated at any time. For example $\mathcal{O} = \phi(\mathbf{x}, t)\phi(\mathbf{0}, 0)$ gives the classical unequal time two point correlator, where $\phi(\mathbf{x}, t)$ is the classical solution defined by the initial conditions $\phi_i(\mathbf{x})$ and $\pi_i(\mathbf{x})$ at $t = t_i$.

Solving the classical theory perturbatively is straightforward. If one is interested in the correlator $\langle\phi(\mathbf{x}, t)\phi(\mathbf{0}, 0)\rangle$, for example, one can choose $t_i = 0$ and solve the classical field equation

$$(\partial_t^2 - \nabla^2 + m^2)\phi = -\frac{1}{6}\lambda\phi^3 \tag{13}$$

with an integral equation:

$$\phi(x, t) = \phi_{free}(x, t) - \frac{\lambda}{6}\int_0^t dt' \int d^3x' G_R(x - x', t - t')\phi^3(x', t') \,. \tag{14}$$

where ϕ_{free} is a solution of the free theory,

$$G_R(x - x', t - t') = \int \frac{d^3k}{(2\pi)^3} e^{i\mathbf{k}\cdot(\mathbf{x}-\mathbf{x}')} \frac{\sin(\omega_k(t - t'))}{\omega_k} \tag{15}$$

is the retarded Greens function, and $\omega_k = \sqrt{k^2 + m^2}$. The iteration of this equation produces the solution for $\phi(x, t)$ to all orders in λ. Of course $\phi_{free}(x, t)$ is easily expressed in terms of $\phi(\mathbf{x}, 0)$ and $\pi(\mathbf{x}, 0)$:

$$\phi_{free}(x, t) = \int \frac{d^3k}{(2\pi)^3} e^{i\mathbf{k}.\mathbf{x}} \left(\phi(\mathbf{k}, 0)\cos(\omega_k t) + \pi(\mathbf{k}, 0)\sin(\omega_k t)/\omega_k\right) \,. \tag{16}$$

To evaluate (12) one expands $e^{-\beta H_{int}}$ in powers of λ, and performs the Gaussian integrations over $\phi(\mathbf{x}, 0)$ and $\pi(\mathbf{x}, 0)$ occurring at each order in λ. These integrals are summarized by the generating functional:

$$\langle e^{\int d^4x \phi_{free}(x)J(x)}\rangle_{\beta,free} = e^{\frac{1}{2}\int d^4x \int d^4x' J(x)G(x,x')J(x)} \tag{17}$$

$$G(x, x') \equiv < \phi_{free}(x)\phi_{free}(x') > = T\int \frac{d^3k}{(2\pi)^3} e^{i\mathbf{k}\cdot(\mathbf{x}-\mathbf{x}')} \frac{\cos(\omega_k t)}{\omega_k^2} \,. \tag{18}$$

To summarize, the interactions occur in two places: first, in $e^{-\beta H}$, which defines the thermal state and determines the equal time correlators, and second, in the classical evolution of the fields between the times of interest in unequal time correlators. The same is true in the quantum theory.

In the quantum theory, one wants to compute the quantum expectation values of operators:

$$\langle\mathcal{O}\rangle_\beta = \frac{\mathrm{Tr}(e^{-\beta H}\mathcal{O})}{\mathrm{Tr}(e^{-\beta H})} \tag{19}$$

where the trace is over any complete set of states, and $\mathcal{O}$ is the product of field operators, expressed in terms of Heisenberg fields. As in the classical theory, one can evaluate this expression in an interaction picture defined at any time (e.g. $t = 0$).

Rewriting (19) in terms of the interaction picture operators $\phi^I(\mathbf{x},t)$ and $U(t) = Te^{-\frac{i}{\hbar}\int_0^t dt' H^I_{int}(t')}$, we have

$$\mathrm{Tr}\left(e^{-\beta H}\frac{1}{2}(\phi^H(\mathbf{x},t)\phi^H(\mathbf{0},0)+\phi^H(\mathbf{0},0)\phi^H(\mathbf{x},t))\right)$$
$$= \frac{1}{2}\sum_i e^{-\beta E_i}\langle i|U(-i\hbar\beta)U^\dagger(t)\phi^I(\mathbf{x},t)U(t)\phi^I(\mathbf{0},0)|i\rangle + \text{c. c.} \qquad (20)$$

where the sum is over a complete set of interaction picture occupation number states. This expression is straightforward to evaluate, by expanding all the U operators in powers of λ and then evaluating the ensuing free field correlators.

To see the connection with the classical theory, note that $U^\dagger(t)\phi^I(\mathbf{x},t)U(t)$ is just the original Heisenberg field, which obeys the classical field equation (13), and as in the classical theory, this may be solved by iterating the integral equation (14), with the identical retarded Greens function. The perturbative expansion of the Heisenberg operator yields this Greens function via $[\phi^I(x,t),\phi^I(x,t')] = i\hbar G_R(x-x',t-t'), t>t'$; the $\hbar$ cancels the $\hbar^{-1}$ in the time evolution operator, to all orders in λ. So the 'dynamical' part of the calculation of unequal time correlators in the classical and quantum theories are actually identical[3]. It is also remarkable that when organized this way, both theories have exactly the same set of Feynman diagrams, it is just the Feynman rules that are different.

Differences arise in two places. First, in the expectation values of the resulting series of free fields. In the quantum theory the generating function is given as in (16) but with $G_{class}(x,x')$ replaced by

$$G_{quantum}(x,x') = \int \frac{d^3k}{(2\pi)^3}e^{i\mathbf{k}.(\mathbf{x}-\mathbf{x}')}\frac{\hbar}{\omega_k}\cos(\omega_k t)\left[\frac{1}{e^{\beta\hbar\omega_k}-1}+\frac{1}{2}\right]. \qquad (21)$$

(This 'thermal Wicks theorem' has been discussed recently by [27] - the simplest way to derive it is to note that the relevant path integral is Gaussian, from which (16) follows. The 'thermal Wicks theorem' is true for any initial density matrix which is Gaussian.). The second difference arises because $U(-i\hbar\beta) = Te^{-\frac{1}{\hbar}\int_0^{\hbar\beta} H_{int}(\tau)}$ is not exactly equal to $e^-\beta H_{int}(0)$. This difference can be attributed to the difference between the quantum and classical (or 'dimensionally reduced') thermal states.

We now see when the classical and quantum results agree. For low frequency bosonic modes at high temperatures $\hbar\omega/T \ll 1$, the occupation number is high and the bracketed expression in Eq. (21) can be expanded in an asymptotic series,

$$\left[\frac{1}{e^{\beta\hbar\omega_k}-1}+\frac{1}{2}\right] = \frac{T}{\hbar\omega_k}+\frac{1}{12}\frac{\hbar\omega_k}{T}+\ldots \qquad (22)$$

[3]except that one must be careful about operator ordering in using the Heisenberg operator equation of motion. The products of operators one gets will not be completely ordering averaged. However, re-arranging their order only introduces commutators which are $O(\hbar)$, which by dimension counting means $O(\hbar\omega/T)$. It turns out that when one asks questions about ordering averaged products of operators, as we do here, these re-ordering corrections actually first appear at second order in $\hbar$, see [26].

and the leading term precisely reproduces the classical Greens function. Note that the usual $\hbar$ in the propagator is cancelled by a $\hbar^{-1}$ in the occupation number. Second, as noted above, $H^I_{int}(\tau)$ is not equal to $H^I_{int}(0)$ - the imaginary time dependence of the free field operators causes a difference in the thermal state corrections. However $H^I_{int}(\tau)$ can be expanded as a Taylor series in τ, and the τ dependent corrections come in the form $\hbar\omega_k\tau < \hbar\omega_k/T$. Thus again for $\hbar\omega/T \ll 1$, the corrections are small [4].

To summarize, as long as one is interested in phenomena which are dominated by low frequency bosonic modes, for which $\hbar\omega/T \ll 1$, the the classical field theory provides a good description. Note that the thermal classical theory contains much more than just tree diagrams - it sums up all loop diagrams as well, in the approximations first that the quantum propagator is replaced by the classical ($\hbar$ independent) piece and second that the thermal state is taken to be that of the 'dimensionally reduced' three dimensional theory.

The above argument works perfectly in a regularized (e.g. lattice) field theory. The only catch in applying it to a continuum field theory is that the condition $\hbar\omega/T \ll 1$ cannot be true for the very high k modes. For large k the quantum and classical propagators are very different, and the ultraviolet behavior of the theory approaches that of the vacuum quantum theory. However, if we are interested in long wavelength correlation functions, these ultraviolet modes will only emerge in diagrams in which there are a few closely spaced vertex insertions, which we should be able to replace with an expansion in local operators. The classical theory will only make sense as a regulated, infrared effective theory with a Lagrangian which takes into account these local, quantum effects. For instance, the couplings will be renormalized, to a scale given roughly by the temperature.

In addition to short distance vacuum corrections, which simply lead to the usual renormalization of the couplings to a scale given roughly by T, there are thermal (non-vacuum) short range corrections, whose form is not restricted by Lorentz invariance because the thermal bath chooses a preferred time direction. There has been intense research into how these effects influence the behavior of the infrared (soft) modes, and it has been shown that the parametrically leading effects can be summarized as a set of "hard thermal loop" effects which can be incorporated into the Lagrangian of the infrared theory [28].

For this reason, Bodeker et. al. proposed to include the hard thermal loop effects in numerical investigations of the classical field theory [29]. In fact, their work shows that they are already included, because the most ultraviolet classical excitations in a (lattice cut off) classical simulation perform the same role as the high frequency thermal excitations in the quantum theory; all that is different from the quantum theory is the shape of the cutoff and the total strength of the hard thermal loop effects. The total strength of the hard thermal loop effects generally cancels in calculations of dynamical properties of the plasma [30], because the hard thermal loops represent

[4] In fact for equal time correlators of ϕ only, these thermal state corrections occur only at order $(\hbar\omega_k/T)^2$, as is seen by writing $U(-i\hbar\beta) \simeq e^{+\beta H_0}e^{-\beta H}$ with (quantum) corrections arising from commutators of H_0 with H_{int}. At first order in $\hbar$ there is only the single commutator, which is odd in π and therefore does not contribute to the correlator.

both a bath of particles against which to scatter, and a bath of particles which screen interactions so that only shorter range scatterings can take place. It is not generally believed that the total number of particles available to contribute to the hard thermal loops affects the infrared dynamics, and if it does, then dynamical properties would show a power law in a (the lattice spacing) dependence. Testing for a small a limit to dynamical properties therefore constitutes a check that the magnitude of hard thermal loops does not matter, or at least that the dynamical property in question converges to a limit in the (parametrically justified) limit of large hard thermal loop contributions. The only remaining concern is that the functional form of the hard thermal loops is incorrect because of cutoff artefacts; but by varying the form of the cutoff one can test for this as well, and at least in the case of the motion of Chern-Simons number it appears that lattice artefacts are small and consistent with zero [22].

Hence, we conclude that the classical theory can be used to examine the thermodynamics of Yang-Mills Higgs theory and allows the study of the infrared dynamics as well, though here there are some legitimate concerns involving hard thermal loops.

3 Numerical implementation of the theory

The numerical implementation of classical, real time Yang-Mills Higgs theory is well developed in the literature [31, 19, 20, 22]. The implementation we use here is identical to that of [19]; we consider the theory at zero Weinberg angle (no $U(1)_Y$) and take as degrees of freedom an SU(2) matrix on every link of a 3+1 dimensional lattice which is toroidal in the 3 space directions but infinite in the time direction, and a fundamental complex scalar at each vertex. The lattice action is

$$\begin{aligned}
\beta_L S &= \beta_L \Big[-\sum_{\Box_s} 1 - \frac{1}{2}\mathrm{Tr} U_{\Box_s} + \frac{1}{(\Delta t)^2}\sum_{\Box_t} 1 - \frac{1}{2}\mathrm{Tr} U_{\Box_t} \\
&- \sum_{x,t}\sum_i \frac{1}{2}(\Phi(x,t) - U_i(x)\Phi(x+i,t))^\dagger(\Phi(x,t) - U_i(x)\Phi(x+i,t)) \\
&+ \frac{1}{(\Delta t)^2}\sum_{x,t}\frac{1}{2}(\Phi(x,t) - U_0(x)\Phi(x,t+\Delta t))^\dagger(\Phi(x,t) - U_0(x)\Phi(x,t+\Delta t)) \\
&- \sum_{x,t}(\frac{m_{H0}^2}{2}\Phi^\dagger\Phi + \frac{\lambda_L}{4}(\Phi^\dagger\Phi)^2)\Big] . \qquad (23)
\end{aligned}$$

We absorb the gauge coupling into the lattice temperature β_L, which is related to the lattice spacing and the continuum temperature through

$$\beta_L = \frac{4}{g^2 a T} . \qquad (24)$$

We also give the Higgs fields the same wave function normalization as the gauge fields, which is natural and computationally convenient. The Higgs field is treated as four independent real entries, and the relation between the lattice value and the

continuum one is

$$\beta_L^2 \Phi^\dagger \Phi = \frac{4}{g^2}\phi^2_{\rm cont} = \frac{8}{g^2}\Phi^\dagger\Phi_{\rm cont} \tag{25}$$

for the normal continuum definitions of ϕ and Φ. With this wave function normalization, the scalar self-coupling λ_L is related to the usual continuum one by

$$\lambda_L = 4\lambda/g^2\,, \tag{26}$$

which is parametrically order 1 if $\lambda \sim g^2$, as is natural from the renormalization structure of the theory. The only small numbers in the classical theory are $1/\beta_L \propto a$ the lattice spacing, and m_H^2 the renormalized Higgs mass squared.

Varying the action with respect to the link in the time direction generates a constraint, analogous to the continuum condition $D_i E_i^a/g^2 = {\rm Re}(\Pi^\dagger i\tau^a\Phi) = \rho$, which is Gauss's law; variation with respect to the space links and the Higgs field components give equations of motion which allow all future times to be determined from two neighboring time slices (provided that these initial conditions satisfy the constraints), once an ambiguity in the time evolution, due to the freedom to change gauge independently at each spacetime point, has been used up by choosing the gauge which always makes the time links $U_0 = I$ the identity.

In practice we keep track of the values of fields on one time slice, and "momenta" $\Pi(t-\Delta t/2) = \Phi(t) - \Phi(t-\Delta t)$ and $E_i^a(t-\Delta t/2) = -1/2{\rm Tr} i\tau^a U_i(t) U_i^\dagger(t-\Delta t)$ (after setting the U_0 to I); as long as E is small, the latter relation can easily be inverted to update U.

We thermalize the system with the algorithm developed in [21]. That is, beginning from an arbitrary initial condition, we repeatedly draw the momenta from the correct thermal distribution (achieved by choosing them as Gaussian random variables, and then orthogonally projecting to the constraint surface) and then evolve the system under the equations of motion for some time, allowing the thermalization to mix with the coordinates U and Φ. The momenta are then discarded and the procedure is repeated, as many times as desired. The algorithm has a time stepsize ambiguity, which we handle as in [22]; the thermalization is only accurate to $O((\Delta t)^2)$, a level which is sufficient because the evolution algorithm is also inaccurate at this level. In this work we always use $\Delta t = 0.05$ in lattice units, which is sufficient to hold stepsize systematics below statistical errors.

As discussed above, a thermalization algorithm for classical Yang-Mills Higgs theory can be considered a canonical ensemble (fixed temperature) Monte-Carlo algorithm for the dimensionally reduced theory. (In fact, except for the Gauss constraint, it exactly resembles the hybrid algorithm of Euclidean lattice gauge theory.) The algorithm is very efficient at exploring the thermodynamics of one phase; but it is very bad at going between the two phases. This is because it must move smoothly from one phase to the other, and mixed phase configurations contain phase boundaries which have positive surface tensions. In the limit of large box size, the suppression of such configurations grows roughly as $\exp(-2L_1L_2/\sigma)$, with L_1 and L_2 the two shortest lengths of the box and σ the surface tension. It is necessary to change phase several times to get good statistics on the free energy difference of the two phases,

and hence to determine the critical temperature, but as the box size grows, it will become essentially impossible for the canonical evolution algorithm to do so; it will only be capable of thoroughly exploring one minimum, but not of comparing the two. For this reason, the literature generally considers a multicanonical ensemble (in which a global reweighting term is added to make mixed phase configurations more favorable but is then accounted for in computing thermal averages of operators) a more powerful technique for exploring the thermodynamics of first order phase transitions.

In fact, properties of the metastable phases, the equilibrium temperature, and virtually all other themodynamic properties can be extracted by using a microcanonical (fixed energy) ensemble. A microcanonical ensemble is achieved by thermalizing the system to some temperature, but then allowing it to evolve under the equations of motion indefinitely, without ever re-randomizing the momenta. The system is strongly ergodic, so for general initial conditions it will thoroughly explore the fixed energy subsurface of phase space. In the large volume limit, this would become approximately equivalent to a canonical ensemble, except that there is a first order phase transition. There is a finite range of energies where the fixed energy equilibrium configuration is mixed phase, and if one can find one mixed phase configuration in this range, then the microcanonical algorithm can use it to thoroughly explore mixed phase configurations, and in particular to extract the phase transition temperature and information about the phase interfaces. Since the whole range of mixed phase configurations occur at a single temperature, the canonical ensemble is not well suited to exploring phase coexistence. This difference between the two ensembles is illustrated in Figure 1.

To exploit this property of the evolution algorithm, it is necessary to find a way to measure temperature during a fixed energy evolution, and to very gradually increase or decrease the energy so that a range of configurations can be explored. If there were no Gauss constraint, it would be easy to measure the temperature. The momenta would be true Gaussian degrees of freedom, and their average energy (averaged over the set of momenta and over time to remove fluctuations) should obey equipartition. The Gauss constraint only mildly complicates this picture. The constraints are linear in the momenta, and remove one Gaussian degree of freedom each. Although they are not local, so we do not know an orthogonal basis for the remaining set of independent Gaussian degrees of freedom, we still know their total number, so the total kinetic energy should equal (number of degrees of freedom=10)$T/2$. Averaging over time removes statistical fluctuations and gives a clean value for the system temperature.

It is also quite easy to gradually change the amount of energy in the system. Our algorithm to do this is to simulate a gradual, adiabatic expansion or contraction of the lattice. All coordinates (U and Φ) are updated as usual, but all momenta E, Π are multiplied by the same factor $(1 + \epsilon\Delta t)$ each time step. The system heats with time constant $1/\epsilon$. If ϵ is negative, the system will cool. Since the Gauss constraint is linear in E and Π, this heating algorithm identically preserves Gauss' Law.

It is also sometimes necessary to make the heating or cooling more local, so that the temperature can be kept uniform even if some phenomenon liberates heat locally. To do this we bin the lattice into boxes or slabs, and measure the temperature in each. Then each box has its momenta multiplied using a different ϵ, chosen to drive

each box independently towards some desired temperature. The algorithm generates small violations of Gauss' Law on the interfaces between boxes, which we remove with the orthogonal projection algorithm presented in [21].

Note that neither of these heating algorithms will keep the system in equilibrium; of course no heating algorithm will. But if they are applied gradually, the system should remain very close to equilibrium (though it will tend to superheat or supercool into metastable phases, as noted earlier).

4 Thermodynamic properties

We are now ready to explore the equilibrium properties of Yang-Mills Higgs theory. We will not attempt a thorough investigation of the strength of the phase transition as a function of λ_L, as very accurate calculations already exist [16, 32]; rather we will investigate how well the microcanonical technique can be applied to determining the various properties of the phase transition. Similarly, we have not attempted to make a small lattice spacing extrapolation; all the data presented below are for $\beta_L \simeq 8$ or 6 and $\lambda_L = 0.20$, which, in the notation of [9], is $x = 0.05$.

4.1 Metastability and hysteresis

The first thing we can investigate is the temperature dependence of order parameters, including metastable branches. We do this by thermalizing a 30^3 lattice with bare Higgs mass squared $m_{H0}^2 = -0.3223$ in lattice units and $\lambda_L = 0.20$ at a temperature above the phase transition temperature, estimated to occur where m_{H0}^2 equals the one loop counterterm,

$$\delta m_H^2 = \frac{(9 + 6\lambda_L)\Sigma}{4\pi\beta_L}\,, \tag{27}$$

which happens when $\beta_L \simeq 8.0$. The system is gradually cooled, and the lattice temperature and order parameters such as $\Phi^\dagger\Phi$ are averaged in time bins longer than the lattice length but much shorter than the full length of the cooling. After the order parameter jumps to the broken phase value, the system is heated back to the original temperature. As a function of temperature, order parameters exhibit hysteresis, returning to the symmetric phase at a higher temperature than they left it. This is the signature of a first order phase transition. The hysteresis curve for $\Phi^\dagger\Phi$, a once smoothed $\Phi^\dagger\Phi$ defined in Appendix B, and the traces of a few sizes of Wilson loops are presented in Figures 2 and 3. Smoothing Φ greatly reduces the contributions from the most ultraviolet fluctuations, but barely touches the infrared fluctuations. We expect that almost all of the value of $\Phi^\dagger\Phi$ in the symmetric phase should arise from ultraviolet fluctuations, which should contribute $\beta_L\Sigma/\pi \simeq 8.1$ to $\Phi^\dagger\Phi\beta_L^2$ [15], so the value of $\Phi^\dagger\Phi$ should be much lower in the symmetric phase after smoothing; but almost all of the difference between phases should be infrared and unaffected by smoothing. Figure 2 verifies this, and also shows that almost all of the random thermal fluctuations in the order parameter are infrared, because the details of the fluctuations in $\Phi^\dagger\Phi$ are almost unchanged by the smoothing. Note also that,

except near the spinodal point, the fluctuations in the symmetric phase value of $\Phi^\dagger\Phi$ are much smaller than in the broken phase; this is because of interference between fluctuations and the condensate in the broken phase. Also note that there is a large correlation between the fluctuations of different sized Wilson loops, and between the fluctuations in Wilson loops and the fluctuations in $\Phi^\dagger\Phi$.

Examining the Wilson loop plots, we see that, in the symmetric phase, traversing a 9×9 loop yields an almost completely random SU(2) phase, so the symmetric phase is disordered on the scale of β_L. In the broken phase traces of Wilson loops fall off more slowly, but 13×13 Wilson loops show almost no order and it cannot be meaningful to speak of anything in a nontrivial representation of SU(2) as having any correlations beyond this scale. Hence the box size was abundantly larger than the longest possible correlation length and the results should represent the infinite volume limit. We also verified this by repeating the run on a 20^3 lattice; the results were the same within error, but the fluctuations were larger because they were not averaged over as much four-volume, so we will not present the results here.

4.2 Equilibrium temperature

The results presented in Figure 2 can be used to determine the jump in $\Phi^\dagger\Phi$ at any temperature for which both phases are reasonably metastable. However, it cannot be used to determine the nucleation rate, because in the early universe the supercooling occurred much more gradually than in any concievable simulation and the true nucleation point occurs when the tunneling probability is too small to observe in a simulation. It also cannot give us the equilibrium temperature, although if we knew the equilibrium temperature we could use the hysteresis plot to find the jump in the order parameter at equilibrium. To get the equilibrium temperature, we must establish phase coexistence in a microcanonical evolution and measure the temperature.

We do this as follows. We thermalize an $N \times N \times 192$ rectangular box with symmetric boundary conditions at the same value of λ_L and m_{H0}^2 used above and $\beta_L = 8.0$. Then we apply a small perturbation to m_{H0}^2, with an amplitude which varies sinusoidally along the long direction of the box. The symmetric phase is favored in one region and the broken phase is favored in another, so a mixed phase configuration is established. The perturbation is then slowly removed, and as it is removed the system is heated or cooled by a thermostat which tries to balance $\int \Phi^\dagger\Phi d^3x$ at a value intermediate between the two phases. Once the perturbation is completely lifted, the system is allowed to evolve for a long time (at least 500 lattice lengths) without any heating or cooling to equilibrate fully in the mixed phase configuration and erase all record of the process by which a mixed configuration was generated. It is then evolved for a long period of time, again without any heating or cooling, during which the energy in kinetic degrees of freedom is averaged and used to establish the equilibrium temperature. We have checked that the box we used was abundantly longer than that required to contain two domain walls and a region of each phase, and that the system remained in the two phase configuration during the whole run. The two phase nature can be seen clearly by averaging $\Phi^\dagger\Phi$, optionally applying several iterations of smoothing, over the two short directions of the lattice and plotting against the

long direction, as shown in Figure 4. The reason that fluctuations in phase boundary positions do not drive the system to one or the other phase is that a fluctuation which expands the broken phase liberates latent heat, which raises the temperature and makes the symmetric phase more favorable, and similarly a fluctuation which expands the symmetric phase absorbs latent heat and makes the broken phase more favorable.

We measured the equilibrium temperature in a $16 \times 16 \times 192$ box and in a $32 \times 32 \times 192$ box; the answers are within errorbars and average to $\beta_L = 8.059 \pm .002$[5]. The jump in the order parameter $\Phi^\dagger\Phi\beta_L^2$ at this temperature, read off the hysteresis plot, is $9.5 \pm .2$. This corresponds to a jump in the continuum order parameter ϕ of $1.54gT$ (g the weak coupling). Two loop perturbation theory predicts a jump of $1.24g$, which is smaller[6]; this might at first seem surprising, considering that the values found by Kajantie et. al. [16] for λ_L on either side of $\lambda_L = 0.2$ are closer to the two loop perturbative value. The reason is that they perform an extrapolation to zero a (infinite β_L) based on data at several values of β_L, whereas the result we quote above is for one value of β_L and contains finite lattice spacing artefacts. Because λ_L is small and the jump in the order parameter is quite sensitive to its value, the most important of these effects may be those which shift the effective value of λ_L. One arises because we have A_0 fields with finite Debye mass squared; if we integrated them out, then they would shift λ_L by [9]

$$\delta\lambda = \frac{-3g^4T}{128\pi m_D} \quad \Rightarrow \quad \delta\lambda_L = \frac{-3}{8\sqrt{5\pi\beta_L\Sigma}} \simeq -0.0188\sqrt{8/\beta_L}\,. \tag{28}$$

There is also a linear in a correction to λ_L arising from one loop diagrams. The one loop contribution to the effective potential is

$$V_1(\phi_0) = \sum \int_{m(\phi=0)}^{m(\phi=\phi_0)} mI(m)dm\,, \tag{29}$$

where the sum is over massive degrees of freedom and $I(m)$, the one loop $3d$ lattice tadpole graph, is computed in [15],

$$I = \frac{\Sigma}{4\pi a} - \frac{m}{4\pi} - \frac{\xi a m^2}{4\pi} + O(a^2)\,, \quad \xi = 0.1529\,. \tag{30}$$

The leading, $1/a$ term generates the linearly divergent mass squared correction, the next term gives the negative cubic term which determines the order of the phase transition, and the am^2 term produces an $O(a)$ correction to λ which, summed over degrees of freedom, is

$$\delta\lambda = \frac{-\xi aT}{4\pi}\left(\frac{9g^4}{16} + 12\lambda^2\right) \quad \Rightarrow \quad \delta\lambda_L = \frac{-\xi}{4\pi\beta_L}(9 + 12\beta_L^2)\,, \tag{31}$$

[5]In the thermalization algorithm, $E(t)$ is drawn from the Gaussian distribution and $E(t+\Delta t/2)$, the value required for the leapfrog algorithm, is determined by a half leapfrog step; but the temperature quoted is the sum of $\sqrt{1-(\Delta t)^2E^2(t+\Delta t/2)}/\Delta t$, so the value we quote will have a weak stepsize dependence.

[6]Here and throughout we use Eq. (34) of [15], with all terms involving m_L dropped, for the two loop effective potential

which equals -0.014 for $\beta_L = 8$. Hence, the simulations described correspond to λ_L of roughly 0.167 rather than 0.2, and the two loop perturbative estimate for ϕ is $1.40g$, quite close to the actual value.

Note that accounting for finite a shifts in λ_L as above does not completely remove finite a or even all linear in a errors, because we have not corrected wave functions or removed high dimension operators. It is probably not profitable to pursue high statistics calculations until the required corrections have been computed.

Also note that the jump in $\Phi^\dagger\Phi$, together with the value for m_{H0}^2, determines the latent heat, as shown in [15]. A more direct measure of the latent heat is the temperature change during the spinodal jump from one phase to the other, which can be looked up on the hysteresis plot (though it must be remembered that the heating or cooling of the system continued during the jump). The value obtained from the jump in temperature is consistent with the latent heat obtained from the jump in $\Phi^\dagger\Phi$.

4.3 Surface tension

Another interesting property of the equilibrium system is the surface tension of the phase interface. The surface tension can be determined from the power spectrum of fluctuations of the interfaces. To understand this, consider a surface with a very large surface tension; since it is taut, it should be flat. But for finite surface tension, the entropy associated with having nonzero fluctuations on the surface prevents it from being perfectly flat. For long wavelength fluctuations, the fluctuation amplitude is small compared to the wavelength, and different fluctuations approximately decouple; on average they are populated according to equipartition. Thus the infrared limit of the power spectrum (square of the Fourier coefficients) of the bubble surface determines the surface tension. The details are given in Appendix B, where we also discuss how we define the bubble wall surface.

To apply the technique discussed in the appendix, we evolved an equilibrated mixed phase configuration for on order 1000 lattice lengths, recording both bubble wall surfaces every 2 lattice lengths of time. Each surface is Fourier transformed, and the square of each Fourier coefficient is averaged over the run. For each value of n^2 there are several independent coefficients (from the real and imaginary parts of one or more Fourier coefficients from two walls), and we average these and take the error bars to be the standard deviation of the mean.

We plot the resulting power spectrum, multiplied by n^2 the square of the Fourier mode number, for a $32 \times 32 \times 192$ lattice at $\beta_L \simeq 8$ and for a $36 \times 36 \times 144$ lattice at $\beta_L \simeq 6$ in Figure 5. This is not a log-log plot; the departure from $1/n^2$ behavior in going from $n^2 = 1$ to $n^2 = 25$ is only on order a factor of two. Part of this departure from strict power law behavior may arise from the smoothing involved in defining the bubble wall surface, and some of it may represent interactions between the high frequency modes on the wall. To make the infinite wavelength extrapolation we fit the data with an exponential; the fit has χ^2/ν of 0.67 and 1.4 for the 32^2 and 36^2 cross section cases and yields surface tensions in physical units of $.0681 \pm .0009 g^4T^3$ and $.0739 \pm .0008 g^4T^3$ respectively. Note that for $\beta_L = 6$ the finite a systematics are

different; the earlier estimate for the correction to λ_L gives $\lambda_L = .160$ in this case, so one should have expected a larger surface tension.

The one loop analytic estimate of the surface tension is

$$\int_0^{\phi_0} d\phi \sqrt{2V_1(\phi)}\,, \tag{32}$$

where V_1 is the one loop effective potential. For $\lambda_L = 0.167$ the result is $.0254 g^4T^3$ and for $\lambda_L = .160$ it is $.028 g^4T^3$. One may also apply the same formula using the two loop effective potential, though this is slightly inconsistent since one is still using the tree level kinetic term without one loop wave function corrections. The results are $.080 g^4T^3$ and $.086 g^4T^3$ respectively. The large difference between the one and two loop perturbative estimates reflects the ϕ^3 dependence of the surface tension. Since the two loop perturbative value for ϕ and the lattice value are quite close, it is not surprising that the two loop surface tension is quite close to the lattice value. The lattice ϕ is larger than the two loop value, but the lattice surface tension is smaller; this may be the beginning of a trend of low surface tensions found in [16], though it is difficult to say until the remaining $O(a)$ effects are accounted for. A lower surface tension is also the direction one would expect from including wave function corrections, as discussed in [33].

We conclude that the microcanonical technique is an efficient and promising way of extracting all interesting thermodynamical properties of the phase transition; it should be further pursued after a more careful accounting of $O(a)$ corrections has been made.

5 Friction on the bubble wall

The previous section merely uses the Hamiltonian evolution of classical Yang-Mills Higgs theory as a microcanonical Monte-Carlo algorithm for thermodynamic investigation, but as stressed in Section 2, the classical Hamiltonian evolution should also give information about dynamics, provided that the physics involved is infrared dominated. This includes two previously elusive phenomena, friction on the bubble wall from infrared bosons and the motion of Chern-Simons number near a moving bubble wall.

5.1 General discussion

The velocity attained by a moving bubble wall during the cosmological electroweak phase transition is one of the key ingredients for models and calculations of baryon number production. Several authors have considered the problem [34, 35, 36, 37, 38, 39, 40, 41, 42, 43], and quite a bit is known. Two effects prevent the bubble wall from "running away" and establish its terminal velocity; frictive effects arising from the departure from equilibrium of massive species due to the motion of the wall, and hydrodynamic effects arising from the liberation of latent heat. The hydrodynamic properties of the plasma are dominated by thermal energy particles, which hold almost

all of the energy and momentum of the plasma, so these effects cannot be studied by classical techniques. Fortunately, except perhaps for energy transfer across the bubble wall by ballistic leptons, the hydrodynamics are well under control [35, 40, 42, 43].

The friction from massive particles depends on a high power of the particle mass, and so the only important particles for consideration are the top quarks and the bosons of the Yang-Mills Higgs system. Friction from top quarks cannot be calculated in the classical theory, but it arises at a higher parametric order than the friction from bosons, where the leading parametric contribution is infrared dominated and should be reproduced in the classical simulations.

To see this, we begin by stating what we mean by the friction. We will only be interested in this paper with the friction in the case that the departure from equilibrium is small, so that a fluctuation dissipation formula can relate it to measurable equilibrium correlators [38]. In this case we define the friction coefficient as

$$\eta \equiv \lim_{P\to 0} \frac{P}{v_w}\,, \tag{33}$$

where v_w is the average velocity of a planar bubble wall when the pressure difference between phases is P. As we will discuss below, this friction coefficient is related to the diffusion constant for the random motion of the equilibrium interface, and converting from lattice units to thermal units establishes the parametric behavior of the classical η as $\eta_{cl} \propto g^6T^4$.

The friction coefficient for the quantum theory can be computed at lowest order in a loopwise expansion from a fluctuation-dissipation theorem [38], and the answer is equivalent to the friction from free scattering, thermal particles on the bubble wall [39], which has been calculated in [36, 37]. The contribution from the 6 transverse W boson modes is

$$\begin{aligned} \eta &= 6\left[\int_0^m \frac{EdE}{4\pi^2}\frac{1}{e^{\beta E}-1}2E^2 \right. \\ &\qquad \left. + \int_m^\infty \frac{EdE}{4\pi^2}\frac{1}{e^{\beta E}-1}\left(2E^2-m^2-2E\sqrt{E^2-m^2}\right)\right] \qquad (34) \\ &\simeq 6\left[\frac{g^3}{32\pi^2}T\phi^3 - \frac{g^4\phi^4}{512\pi^2}\left(\frac{7}{4}+\ln\frac{8\pi T}{g\phi}-\gamma_E\right)\right]\,, \qquad (35) \end{aligned}$$

where the first integral arises from particles which scatter from the wall and the second is from particles which fly over the wall from each side. If we make the approximation $1/(\exp(\beta E)-1) \simeq (1/\beta E)$, which is precisely the classical approximation to the Bose-Einstein population factor, then the integrals give precisely the first $O(g^3\phi^3)$ term. Hence we can understand the result as a classical part, which (recalling that $\phi \simeq gT$) is order g^6T^4, plus a correction which is $O(g^8 \ln 1/g)$. The most important point is that the result is totally dominated by the infrared contribution, and extending the classical approximation for the Bose distribution out to arbitrarily large momenta only makes a parametrically suppressed error; hence the friction from bosons is (at leading parametric order) an infrared, classical effect. This means, of course, that

the loopwise expansion will be unreliable, because the infrared is strongly coupled; instead we should use classical real time simulations to determine the friction.

For the fermions, Eq. (34) applies but with the Bose-Einstein statistics replaced by Fermi-Dirac statistics $1/(\exp(\beta E)+1)$ (and of course the 6 replaced by a 12). The resulting friction is

$$\eta \simeq 12 \left[\frac{g_Y^4 \phi^4}{128\pi^2} \left(\frac{7}{4} + \ln \frac{\sqrt{2}\pi T}{g_Y \phi} - \gamma_E \right) \right] , \tag{36}$$

which begins at $O(g^8 \ln 1/g)$. Friction from top quarks is parametrically suppressed and will not appear in the classical theory, which is obvious because the classical theory is purely bosonic. The top quark contribution to friction may still be significant, simply because it depends on g_Y^4 and g_Y is numerically much larger than g. The absence of a large infrared contribution should also make the top quark friction computable, although the naive perturbative series must be resummed into Boltzmann equations to account for on-shell near singularities [44] and may then require simplifying analytical approximations to make the calculation feasible [41, 42].

Fortunately, most of the top quark friction arises from the small departure from equilibrium of thermal energy particles; because Fermi statistics are well behaved in the infrared, the departure from equilibrium of top quarks will have a small (parametrically suppressed) influence on the infrared bosonic sector. The two frictions should be additive with $O(\alpha)$ error, and an investigation of the friction in the bosonic theory is well motivated.

5.2 Fluctuation dissipation relation

As mentioned above, the $O(g^6)$ contribution to the friction coefficient can be computed in the limit of a small departure from equilibrium by a fluctuation dissipation argument, as follows. Consider an infinite square tube of cross section A, filled with classical Yang-Mills Higgs plasma at the equilibrium temperature. Two semi-infinite regions of definite phase are separated by a domain wall. Because the system has translational invariance, for times much greater than any thermalization time in the plasma the position x of this wall will diffuse,

$$\lim_{t\to\infty} \frac{\langle (x(t)-x(0))^2 \rangle}{t} = D_x \, , \tag{37}$$

with D_x the diffusion constant for x. Hence, the probability that, starting from $x(0)$ at time 0, one will arrive at $x(t)$ at time t, which we call $\mathcal{P}(x(t), x(0), t)$, satisfies

$$\int dx(t) \mathcal{P}(x(t), x(0), t)(x(t)-x(0))^2 = |t| D_x \, . \tag{38}$$

Now suppose that we exert a very small force $f(x) = -V'(x)$ on the bubble wall. We choose V' to be constant in a large neighborhood of the origin, although V eventually turns up so that it is bounded from below and goes to infinity at $x \to \pm\infty$. At leading order the hopping probability will be modified by an offset,

$$\int dx(t) \mathcal{P}_f(x(t), x(0), t)(x(t)-x(0)) = \langle x(t)-x(0) \rangle = Cft = v_w(f) t \tag{39}$$

with C a constant to be determined. Also, the equilibrium probability distribution of x will be multiplied by a Boltzmann factor $\exp(-V/T) = \exp(fx/T) \simeq 1 + fx/T + (fx)^2/2T^2$. Starting with a thermal distribution of wall positions at time $t = 0$, the probability that the wall should be at position $x(t) = 0$ at time t, relative to its probability for starting there, is

$$1 = \int dx(0) \mathcal{P}_f(0, x(0), t) \left(1 + \frac{fx(0)}{T} + \frac{x(0)^2 f^2}{2T^2}\right) = 1 - \frac{Cf^2 t}{T} + \frac{D_x f^2 t}{2T^2}\,, \qquad (40)$$

and hence

$$C = \frac{D_x}{2T}\,. \qquad (41)$$

The pressure on the wall is $P = f/A$, so the friction coefficient is

$$\eta = \frac{P}{v_w} = \frac{P}{fC} = \frac{2T}{D_x A}\,. \qquad (42)$$

In physical units,

$$D_{x\ \mathrm{phys}} = \frac{4 D_{x\ \mathrm{latt}}}{g^2 \beta_L T} \qquad \text{and} \qquad A_{\mathrm{phys}} = \frac{16 A_{\mathrm{latt}}}{g^4 \beta_L^2 T^2}\,, \qquad (43)$$

so $\eta \propto g^6 T^4$, as stated above. To compute the bosonic contribution to the friction coefficient at leading parametric order it is then only necessary to determine $D_x A$ for a bubble wall in a classical simulation.

It is necessary to make a few changes to the above ideas to implement them in a realistic simulation. The simulation occurs in a box with symmetric boundary conditions; there are two bubble surfaces, and there is a slight mutual interaction between them, depending on their separation; for instance, the motion of one wall releases latent heat, which slightly changes the temperature and thereby induces a response from the other wall; so even if each wall's position can be described by a single coordinate, the motion of the two coordinates will be interdependent. The interdependences appear in the motion of the difference of the wall positions, but translational invariance ensures diffusive motion of the average of the wall coordinates. The above arguments apply, except that the force f must be the total force on both walls, and D should be computed for the average coordinate. The same final expression holds, except that A now represents the sum of the areas of the two walls, twice the cross section of the box. In terms of the cross-section of the box and the diffusion rate of the average coordinate D_{av},

$$\eta = \frac{T}{D_{\mathrm{av}} A}\,. \qquad (44)$$

5.3 Numerical results

We determine the wall position as follows. Every few lattice lengths in time, we average $\Phi^\dagger \Phi$ over the short directions of a long rectangular lattice, producing a c-number function of the long direction. this is smoothed with a Gaussian broad enough

lattice size	β_L	t (lattice units)	$D_{\rm av}$ (lattice units)	η
$16^2 \times 192$	8	1100	1.21 ± 0.24	$.026 \pm .005 g^6T^4$
$32^2 \times 192$	8	640	$.25 \pm 0.05$	$.031 \pm .006 g^6T^4$
$36^2 \times 144$	6	674	$.095 \pm 0.015$	$.027 \pm .004 g^6T^4$

Table 1: Data from computing the friction on the bubble wall. Three runs on three lattice sizes and at two lattice coarsenesses are within error.

to make the phases very clearly distinct but well narrower than the wall. For $\beta_L = 8$ and $\lambda_L = 0.2$ we found $\sigma = 3$ lattice units sufficient, but for larger λ_L where the phase transition is weaker the smoothing would need to be stronger (and the cross-section of the box would need to be wider). We set a threshold at some fraction of the way between the average broken phase value and the average symmetric phase value of $\Phi^\dagger\Phi$ (typically 30%) and, starting at the point of minimum $\Phi^\dagger\Phi$, move out in either direction and identify the wall as the first point where the threshold is exceeded. This works well because, as noted earlier, the fluctuations in $\Phi^\dagger\Phi$ are much smaller in the symmetric phase than in the broken phase.

In Figure 6 we plot the average of the positions of the two walls in a $16 \times 16 \times 192$ box. The data are taken every 5 lattice lengths for a period of 1100 lattice lengths. We extract a diffusion constant from this data by the method discussed in Appendix A, which uses the fact that the coefficients of a sine transform of a Brownian process are independent and Gaussian, with variance $\propto 1/k^2$. The power spectrum is plotted in Figure 7, which clearly shows this powerlaw behavior. Results for this run, for a 640 lattice length run in a $32 \times 32 \times 192$ box, and for a 674 lattice length run in a $36 \times 36 \times 144$ box at $\beta_L = 6$, are presented in Table 1. In each case several (order 10) of the lowest frequency Fourier modes were removed, as discussed below, and around 100 of the next lowest modes were used; all higher frequency modes, which are more polluted by small errors in the wall finding algorithm and which may contain physics on time scales too short for the diffusion description to be valid, are also excluded. We checked that 50% changes to these cuts did not significantly affect the results. The error bars reflect the quality of the fit, see Appendix A, and are typically twice the change resulting from a 50% change in the cuts. The runs are mutually consistent, which is a good test since they were performed on lattices of different sizes and coarsenesses. For comparison, the friction expected from the one loop (free scattering) estimate, from transverse W bosons alone, and using the lattice value of $\phi = 1.54g$, is $.069g^6T^4$, larger by a factor of about 2.5. One expected the free particle estimate to exaggerate the friction, because scatterings will thermalize the particles as they reflect from the wall, reducing the friction; but the amplitude of this reduction could not previously be calculated reliably.

We should mention a serious note of caution in establishing these results and in measuring the friction on a bubble wall in a classical simulation. This has to do with hydrodynamics. As noted earlier, the liberation of latent heat by a moving bubble wall raises the temperature of the plasma locally, and the heat is redistributed by the plasma. The temperature at the bubble wall is generically elevated with respect to the temperature at the time the bubble nucleated, slowing the wall in a way which

cannot strictly be said to be frictional. In the quantum system heat is transported by hydrodynamic waves which travel at the speed of sound $v_s = 1/\sqrt{3}$, and for an isolated, spherical bubble, the dissipation of heat into the surrounding medium is efficient if the wall velocity is small.

Latent heat is also liberated in the classical lattice system, but the specifics of the hydrodynamics are cutoff dependent and qualitatively different. For instance, in physical units the heat capacity of the classical plasma increases with inverse lattice spacing as a^{-3}, while the latent heat depends on a^{-1}; so the relation between the latent heat and the energy drop between equilibrium and nucleation depends on a. Worse, heat is not conveyed on the lattice by bulk hydrodynamic flow; it travels diffusively. The reason is that the lattice does not respect momentum conservation; while momentum is approximately conserved for interactions between infrared modes, many ultraviolet modes obey dispersion relations in which adding momentum accelerates the mode in the opposite direction of the applied momentum. Hence, scatterings cause momentum to be lost into the lattice, and bulk flows tend to come to a stop; on large length scales heat dissipates rather than flowing hydrodynamically. We have verified this numerically by heating the lattice system inhomogeneously so as to excite the fundamental standing wave; the amplitude of the standing wave decays rather than oscillates.

The problem lies in preventing the hydrodynamic response of the classical fluid from contributing to the observed friction. In the case of the diffusion rate mentioned above, this becomes a problem for the very low frequency Fourier modes. The latent heat liberated by the motion of the wall tends to sit on top of the wall, diffusing away only slowly, so there is a very long term "memory effect" inducing negative correlations in the wall motion. In Figure 5 we see that the most infrared sine transform coefficients do indeed fall off the power law curve; this is why it is necessary to drop the most infrared coefficients from the analysis of the diffusion constant. Between the low frequency coefficients which must be removed and the high frequency coefficients which do not show diffusive behavior there is a sizeable fiducial range, as we established by moving the cuts in and out on either side by 50% and finding little difference to the determined diffusion rate, as discussed above. The cut for $\beta_L = 6$ had to be sharper because the heat capacity is smaller compared to the latent heat in that case.

Another way of measuring the infrared contribution to the bubble wall friction is to supercool the system in the symmetric phase and produce a small region of broken phase by some means, for instance by briefly making m_{H0}^2 more negative in a narrow region, or by starting with a mixed phase configuration and applying the cooling very abruptly. One then directly measures the velocity at which the bubble walls move and sweep up the symmetric phase, averaging over several repitions with different initial conditions to determine and improve statistics. This technique has the advantage that it does not rely on a linear approximation, which may not be very good if the departure from equilibrium is large; but the latent heat poses a problem for this technique. For the lattice coarseness and value of λ_L used in this paper, the temperature rise due to the liberation of latent heat is comparable to the supercooling, as can be seen from how much the temperature jumps on changing

phase in the hysteresis plots, see Figure 2. Another problem is that, if the departure from linear response really is important, then the frictive pressure may not be linear in v_w, and it becomes more difficult to add the effects of the top quark and the W boson.

We end this section by commenting on possible ways around the hydrodynamics problem. One way is to work on a much finer lattice, so that the heat capacity is large enough to soak up the latent heat without much effect. The obvious disadvantage is that this technique is numerically expensive. Alternately, one could add extra fundamental representation, massive scalars to the theory to serve as an additional heat reservoir. If their masses are chosen large enough then they will have little effect on the infrared physics. They would also tend to raise the Debye screening mass, which might be desirable. As long as they had no coupling to the Higgs boson, one would not expect them to contribute to the friction, except by their interactions with the other particles. A final possible solution is to turn on a very weak Langevin noise and damping term. The technology for doing this in a gauge invariant way was worked out in [45]. As a thermalization algorithm the technique is non-optimal because it thermalizes the infrared modes much more slowly than the ultraviolet ones; but for this application that is a blessing, since one wants to absorb the heat going into the ultraviolet excitations without interfering with the correct infrared dynamics. The main disadvantage is that the Langevin term makes the evolution canonical, rather than microcanonical, so the two phase configuration would be unstable; but in a large enough box it would take a long time for the walls to diffuse into each other. We will not pursue any of these techniques here.

6 Chern-Simons number motion on the bubble wall

Another question which the real time technique can answer is how the system responds to a chemical potential or other driving force for the motion of Chern-Simons number N_{CS}. This is directly relevant to the study of baryon number violation because the axial anomaly relates the motion of baryon number to the motion of N_{CS}. In fact the classical technique was originally proposed to investigate this question [17], and since then it has been used to investigate N_{CS} violation in Yang-Mills theory [20, 21, 22], in the symmetric phase of Yang-Mills Higgs theory [18, 19], and in the broken phase of Yang-Mills Higgs theory [23, 46]. It has yet to be applied to perhaps the most relevant problem, which is the rate of N_{CS} motion in the out of equilibrium environment of a moving bubble wall during the phase transition. The study of mechanisms for baryon number violation at the electroweak phase transition is the study of how the out of equilibrium phase transition physics can induce in the infrared bosonic effective theory CP violating operators. To convert this information into a baryon number abundance we must understand how N_{CS} responds to these operators.

Turok and Zadrozny [5] and McLerran et. al. [6] take the fermions to be in equilibrium and integrate them out, and then try to investigate how the resulting CP violating operators will influence the out of equilibrium decay of gauge field configurations as they are swept onto the wall; but for lack of quantitative tools

they were forced to make only qualitative or parametric estimates (see also [47]). More recently work has focused on how the transport of fermions can carry CP violation away from the bubble wall [7], [50], into the symmetric phase. One of the main motivations for examining the transport mechanism was the worry that baryon number violation on the wall would be strongly suppressed except for at the very leading edge [51], [7], [49], by the turning on of the sphaleron mass. Thus a chemical potential inside the wall would be ineffective. But it remains to be shown whether this picture, based on viewing the baryon number violation as a completely local, quasiequilibrium process, is correct, or whether decaying gauge field configurations swept up onto a bubble wall can still respond to CP violating effects on the wall to produce N_{CS} change. In this chapter we will focus on this question.

To answer it we need to apply a chemical potential for N_{CS} on the lattice, as otherwise we cannot create a CP violating bias[7]. The technology for doing this has recently been worked out for Yang-Mills theory [21], and it is straightforward to extend it to Yang-Mills Higgs theory. We briefly review the method in Appendix A, and extend it to Yang-Mills Higgs theory. For a complete exposition see [21, 22].

The only problem in applying a chemical potential for N_{CS} in Yang-Mills Higgs theory is that the rate of N_{CS} motion (or the rate of N_{CS} diffusion when no chemical potential is applied) is slightly contaminated by ultraviolet lattice artefacts; in the broken phase these effects contribute about 1/10 of the symmetric phase rate to the response. We give evidence that this rate is an ultraviolet lattice artefact in Appendix A. The consequence of this problem is that we must observe a rate of N_{CS} motion well above 1/10 the symmetric phase response rate before we know that it corresponds to genuine infrared processes and not to spurious ultraviolet physics.

With this in mind, we set out to investigate how $\dot{N}_{CS}$ interpolates between the symmetric phase value and the broken phase value across a bubble wall, when there is a spatially uniform chemical potential for N_{CS} in both phases. We do this first in equilibrium. We take a mixed phase configuration with about equal volumes of broken and symmetric phases, in a $16 \times 16 \times 192$ box at the equilibrium temperature and the values of $\lambda_L = 0.2$, $m_{H0} = -.3223$ generally used in this paper. We compute $\dot{N}_{CS}$ at each lattice point and bin it according to its distance from the bubble wall. This means that we find the bubble wall surfaces by the algorithm described in Appendix B, and for each point in the plasma we find the minimum vertical distance to a bubble wall, and add $\dot{N}_{CS}$ to a bin corresponding to that distance, considered positive if the point is on the broken phase side of the wall and negative if it is on the symmetric phase side. Binning this way accounts for the fact that the wall is an uneven surface. We also bin $\Phi^\dagger\Phi$, unsmoothed, using the same rule; this gives a bubble wall profile.

The results for the equilibrium case with a space independent chemical potential are presented in Figure 8. The $\dot{N}_{CS}$ results have been smoothed with a Gaussian

[7]Another possibility is to put CP violating high dimension operators, such as $\Phi^\dagger\Phi E \cdot B$, in the action; although such terms cannot bias N_{CS} in equilibrium, the shift in $\Phi^\dagger\Phi$ during the phase transition will bias topology change. However, implementing such operators makes evolving the system much more complicated, because the update rule becomes nondiagonal in the natural basis of degrees of freedom; also any nonrenormalizeable operator has much more influence on the ultraviolet behavior of the lattice system than on the infrared, which is potentially dangerous.

envelope of width $\sigma = 3$ lattice units to eliminate white noise fluctuations, while the $\Phi^\dagger\Phi$ plot is completely unsmoothed; its smoothness arises from averaging over a long time (approximately 4000 lattice lengths) and over the area of the bubble walls. What we see in these plots is that, in equilibrium, the response to a chemical potential falls off abruptly just inside the bubble wall, and sphaleron events are suppressed in most of the interior of the wall, as well as behind it.

Next we consider the out of equilibrium case. We produce a series of initial conditions by evolving a mixed phase, equilibrium configuration through a series of short ($t = 10$ lattice unit) Hamiltonian trajectories. The starting configuration contains mainly symmetric phase, so the broken phase can expand for some distance before the walls meet. For each initial condition, we evolve it using the "local thermostat" discussed in Section 3 to drive the temperature to a point midway between equilibrium and the spinodal point; we also turn on a global chemical potential for N_{CS}. After waiting about $t = 20$ lattice units for the system to achieve a steady state, we begin to record $\dot{N}_{CS}$ and $\Phi^\dagger\Phi$, binning according to proximity to the bubble wall. We discontinue the evolution well before the bubble walls meet.

The wall shape for the out of equilibrium case, and the motion of N_{CS} in this case, with a constant chemical potential, are presented in Figure 9. The conclusion is similar to the case of the wall at rest; baryon number shuts off some short distance into the bubble wall.

We also investigate the case where the chemical potential exists only on the bubble wall. We could do this by adding a nonrenormalizeable operator $\Phi^\dagger\Phi E \cdot B$ to the action, which closely resembles an operator which would arise in the two Higgs doublet model. However there are serious technical difficulties with adding such a term; it significantly modifies the ultraviolet dynamics, and it renders the update rule nondiagonal. Instead we will "mock up" the effect of this term. First, we measure the averaged dependence of $\Phi^\dagger\Phi$ on distance from the bubble wall, which is shown in Figure 9. Now for each point in the plasma, we find the vertical distance to the nearest bubble wall, and apply a chemical potential at that point which is proportional to the derivative of the wall profile in Figure 9 at that value. The chemical potential is then only nonzero on the wall, and in a way which mimics $d(\Phi^\dagger\Phi)/dz$, which would be $\propto d(\Phi^\dagger\Phi)/dt$ for steady motion of the bubble wall.

We have performed a series of runs with a chemical potential which is only nonzero "on the wall". The bubble wall shape and the average of $\dot{N}_{CS}$ for each run are plotted in Figure 10. The figure shows that N_{CS} is generated in the interior of the bubble wall, where the chemical potential is being applied, but it is destroyed in a region immediately to either side. This is not a fluctuation due to insufficient statistics; if the data set is split in four, each quarter shows the same morphology. The rate of baryon number generation within the hump itself is, in the dimensionless units discussed in Appendix A,

$$\frac{(\beta_L\pi)^4 \int_{\rm hump} \dot{N}_{CS} d^3x dt}{\int \beta_L \mu(x,t) d^3x dt} = 0.225\,. \tag{45}$$

However, when one integrates over the full simulation volume, including the regions

to either side of the bubble wall where $\dot{N}_{CS}$ is negative, one finds

$$\frac{(\beta_L \pi)^4 \int \dot{N}_{CS} d^3x dt}{\int \beta_L \mu(x,t) d^3x dt} = 0.091 \pm 0.025\,. \tag{46}$$

The error bar on the latter number is estimated assuming the error is from diffusion of N_{CS} in the symmetric phase volume in the simulation, and is consistent with the error bar from statistics between runs. the final result is larger than the expected "UV artefact rate" of $\kappa_{\rm UV\ artefact} \simeq 0.055$ (see Appendix A), so one might conclude that there is a net infrared generation of N_{CS} from the chemical potential; however the statistical significance is not very good, and the generation is about an order of magnitude less efficient than in the symmetric phase.

Why is there a bump with a dip on either side, and how can the system respond to a chemical potential on the wall? Recall why a chemical potential should not induce baryon number violation in the broken phase. If a chemical potential is turned on briefly, it will push the gauge fields in the direction which generates baryon number, and, briefly, N_{CS} will be generated. However, the fields will respond elastically to this impulse–after oscillating in the direction of greater N_{CS} they will "bounce back" to the previous value of N_{CS}. The temporal response to an impulse of chemical potential will then be a forward surge in N_{CS} followed by a resotration to the original value. (We have tested this statement by tracking N_{CS} after such an impulse.) Now the gauge fields also propagate, so if a chemical potential is applied in a spatially nonuniform way, the relaxation to the former value of N_{CS} may take place not where the chemical potential was applied, but nearby. This would explain the generation of N_{CS} on the wall and the destruction of N_{CS} immediately to each side. In the case of the moving wall, some of the "excited" gauge field modes relax inside the symmetric phase, because they propagate there. Once in the symmetric phase, their behavior can be different–without a Higgs condensate present, the most infrared modes may no longer be oscillatory and will not relax as much as they would have, so the deficit in $\dot{N}_{CS}$ on the sides of the wall need not be as large as the production on the wall. The infrared gauge fields themselves can serve to transport the CP violation on the bubble wall to the symmetric phase, where it can lead to baryon number nonconservation. However, our data show that this is quite an inefficient mechanism.

In a previous draft of this paper we found a considerably larger effect from chemical potential on the bubble wall. However, in the evolutions used for those results we were insufficiently careful to stop runs well before the bubble walls met; sometimes they would begin to collide, causing the bubble wall finding algorithm to go awry, and possibly leading to the application of chemical potential inside the symmetric phase rather than on the bubble wall surface. For the runs presented here we were more careful; the new runs also represent about 3 times the cumulative evolution time (totaling $t = 14000$ lattice units).

7 Conclusion

We have reviewed the fact that the thermodynamics of quantum Yang-Mills Higgs theory coincides, in the approximation of dimensional reduction, with the thermodynamics of the classical theory, and shown how this can turn the real time evolution of the classical theory into a powerful microcanonical Monte-Carlo algorithm. We used the algorithm, for Higgs potential parameters corresponding to a tree level vacuum Higgs mass of $\simeq 50$GeV, to investigate the phase diagram, including both metastable branches, and to find the equilibrium temperature. We also developed and applied technology for finding the equilibrium surface tension by microcanonical techniques.

Further, we have strengthened the argument that the dynamics, as well as the thermodynamics, of the infrared can be approximated with classical field theory; the errors should be parametrically suppressed (order α_W) for phenomena which are truly infrared dominated. This is a consequence of the weakly coupled nature of the theory; the physics can only become nonperturbative by becoming classical. We were thus able to compute to leading parametric order the friction from bosons on a moving bubble wall in the near equilibrium limit, and to investigate the physics of baryon number violation out of equilibrium in the presence of a moving bubble wall. We have found that the friction from infrared bosons is smaller than that from transverse W bosons in the free scattering limit by a factor of $2-3$, and baryon number violating processes proceed some distance into the bubble wall but stop well short of the broken phase.

The classical method opens all thermodynamic and dynamical properties which are dominated by the infrared bosonic sector to reasonably accurate calculation. To pursue the thermodynamics with good accuracy it will be necessary either to apply a great deal of computer time, or to make a thorough investigation of linear in a corrections. To improve the accuracy and reliability of the dynamical calculations it will be useful in addition to find some way to properly represent hydrodynamic effects on the lattice. It may also be possible to integrate out the A_0 field, so the large Debye mass limit is obtained without necessitating very fine lattices.

We are hopeful that such improvements in accuracy can be achieved, making it practical to use the techniques developed here at a wide range of Higgs masses and for interesting extensions of the Minimal Standard Model, including a second light Higgs doublet and a light stop squark.

Acknowledgements

We would like to express our gratitude to Mark Alford, Peter Lepage, Ron Horgan, Chris Barnes, and Alex Krasnitz for useful conversations. GM would like to thank DAMTP, Cambridge for hospitality. GM was supported under NSF contract PHY90-21984, and NT was supported by PPARC, UK, and a startup grant from Cambridge University. The code used in this paper is written in c, and is reasonably user friendly and well documented; it is free on request to GM.

A N_{CS} in Yang-Mills Higgs theory

Two quantities can be used to characterize baryon number violation in classical Yang-Mills Higgs theory; the diffusion rate of N_{CS}, and $\dot{N}_{CS}$ when there is a chemical potential for N_{CS} added to the Hamiltonian. In the large volume, long time limit these quantities can be characterized by two rates,

$$\Gamma_d \equiv \lim_{t\to\infty} \frac{\langle (N_{CS}(t) - N_{CS}(0))^2 \rangle}{Vt} \quad \text{and} \quad \Gamma_\mu \equiv \lim_{\mu\to 0} \frac{\dot{N}_{CS} T}{\mu V t}\,, \tag{47}$$

which satisfy a fluctuation dissipation relation, $\Gamma_d = 2\Gamma_\mu$, derived in [52] and further discussed in [53, 21]. It is also interesting to know $\dot{N}_{CS}$ for $\mu \gg T$; if $\dot{N}_{CS}$ rises much faster than linearly in μ it indicates that the motion of N_{CS} is obstructed by a substantial free energy barrier; for Yang-Mills theory $\dot{N}_{CS}$ turns out to be very linear so there is no free energy barrier [21].

The technology for computing N_{CS} as a function of time in Yang-Mills Higgs theory, in the absence of a chemical potential, was developed in [19, 20]; we will give only the most cursory review here. Instead this appendix will concentrate on how best to extract a diffusion constant from the diffusive trajectory of N_{CS}, and then on how to extend the chemical potential method developed in [21] to the case of Yang-Mills Higgs theory. We will then investigate N_{CS} motion in the symmetric and broken phases, using both techniques, and present three pieces of evidence that the rate we establish in the broken phase arises from spurious ultraviolet effects.

A.1 Finding a diffusion rate

Suppose we know some quantity z as a function of time t between an initial time 0 and a final time t_f. We believe that it should exhibit Brownian motion, and we want to determine the diffusion constant Γ, defined as $\langle (z(t_1) - z(t_2))^2 \rangle = \Gamma |t_1 - t_2|$. One method, used in [20], is to compute

$$\mathrm{lag}(t_1) \equiv \int_0^{t_f - t_1} (z(t + t_1) - z(t))^2 dt \tag{48}$$

for many values of t_1 and to fit the result to a straight line. While this method works, the fitting is complicated by the large correlations between $\mathrm{lag}(t)$ for different values of t.

We advocate an alternate method in which one sine transforms z and makes a likelihood analysis of the transform coefficients. The analysis is simpler because the sine transform coefficients are independent; and the likelihood analysis is probably optimal in the sense of statistical power.

We begin by redefining $z(t)$ as $z(t) - z(0)$; then

$$\langle z(t_1) z(t_2) \rangle = \Gamma \min(t_1, t_2)\,. \tag{49}$$

Defining the sine transform coefficient

$$\tilde{z}_n = \int_0^{t_f} \frac{dt}{t_f} z(t) \sin\left(\frac{n\pi t}{2t_f}\right) \qquad n = 1, 3, 5, 7 \ldots \tag{50}$$

we quickly find

$$\langle \tilde{z}_n \tilde{z}_m \rangle = \int_0^{t_f} \frac{dt_1}{t_f} \int_0^{t_f} \frac{dt_2}{t_f} \sin\left(\frac{n\pi t_1}{2t_f}\right) \sin\left(\frac{n\pi t_2}{2t_f}\right) \Gamma \min(t_1, t_2) \tag{51}$$

$$= \frac{2\Gamma t_f}{mn\pi^2} \delta_{mn} \,. \tag{52}$$

The sine transform coefficients are independent, with variance $2\Gamma t_f/(n\pi)^2$. They will also be Gaussian distributed. We can see that the sines used form a complete set by extending z as an odd function about the origin and an even function about t_f.

In the case of interest, z will only be known at discrete values of t, and the integrals above represent the corresponding sums. z will also often be contaminated by white noise–this was proven in the case of Yang-Mills theory by Ambjorn and Krasnitz, by considering the Abelian approximation to the ultraviolet modes of the theory [20]–which will introduce a constant times δ_{mn} into Eq. (52). The value of this constant is uninteresting, but its presence means that the ultraviolet coefficients do not carry information about Γ, which can only be determined with finite precision. Any other non-Brownian correction to the ultraviolet physics, as we expect for instance in extracting the diffusion constant for the bubble wall motion considered in Section 5, also makes the ultraviolet data useless.

The remaining question is how, given a set of Gaussian distributed coefficients $\tilde{z}_n$, $n = 1, 3, 5 \ldots$, satisfying

$$\langle \tilde{z}_n^2 \rangle = \frac{A}{n^2} + B \,, \tag{53}$$

to extract A and its errorbars. If we assume a uniform prior for the values of A and B, then Bayes' theorem gives the likelihood of values A and B as

$$\mathcal{P}(A, B) \propto \prod_{n=1,3,\ldots} \frac{\exp(-\tilde{x}_n^2/2\sigma_n^2)}{\sqrt{2\pi}\sigma_n} \,, \qquad \sigma_n^2 = \frac{A}{n^2} + B \,. \tag{54}$$

The best value of (A, B) is that which maximizes this likelihood function. If the likelihood function is sharply peaked and there is a neighborhood of the maximum which contains almost all of the probability, and in which $\ln \mathcal{P}$ is well approximated by a quadratic form, then the likelihood will be approximately Gaussian distributed with an error matrix which is the inverse of the quadratic form. If there is enough data to make a strong determination of A and B then this is generally the case. This is how we determine best fits and errors for Brownian processes in this paper, and it will allow us to find the N_{CS} diffusion rate in either electroweak phase.

A.2 Chemical potential method in Yang-Mills Higgs theory

It is useful to be able to measure the response of N_{CS} to a chemical potential. This idea was first investigated for Yang-Mills Higgs theory by Ambjorn et. al. [19], who encountered technical difficulties; these were overcome for Yang-Mills theory in [21]. Here we briefly extend the method developed there to Yang-Mills Higgs theory.

The first step is to define an (adjoint valued vector) magnetic field B; the appropriate choice is [20]

$$B_i^a(x) = \frac{1}{8}\sum_{4\Box_{x,jk}} \frac{1}{2}\mathrm{Tr} - i\tau^a U_\Box + \frac{1}{8}\sum_{4\Box_{x+i,jk}} \frac{1}{2}\mathrm{Tr} - iU_i(x)\tau^a U_i^\dagger(x) U_\Box \tag{55}$$

where each sum is over 4 plaquettes orthogonal to the x, i link, $U_\Box$ is the product of links around that plaquette beginning and ending on the link, and the two sums are for the basepoint and endpoint of the link. The $U_i(x)$ and $U_i^\dagger(x)$ in the second term parallel transport $U_\Box$ to the basepoint of the link. $\dot{N}_{CS}$ is then defined as

$$2\pi^2 \dot{N}_{CS} = \sum_{x,i} E_i^a B_i^a \equiv E \cdot B \tag{56}$$

where we have displayed the definition of inner product for adjoint vector fields. These two definitions are already sufficient for tracking the (diffusive) motion of N_{CS} in the absence of a chemical potential.

Next we see how to apply a chemical potential for N_{CS}. First consider Yang-Mills theory. On the lattice it is not necessarily true that

$$0 = \nabla \cdot B(x) \equiv \sum_i (B_i(x) - U_i^\dagger(x-i) B_i(x-i) U_i(x-i)) \tag{57}$$

which means that if, for some reason, the Gauss constraint were not actually obeyed, $\dot{N}_{CS}$ would depend on the size of the violation. To understand this point, suppose that we knew an orthonormal basis for adjoint vector fields which partitions into basis elements which are linear combinations of the constraints (which can be constructed by taking the gradients of adjoint valued scalar fields) and basis elements with zero divergence. Call the projection of the electric field into the former subset E^c (c for constraint) and the projection into the latter subset E^*. The Gauss constraint is the condition $E^c = 0$, and the E^* are the dynamical degrees of freedom. Similarly, B partitions into B^c and B^*, and the above point is that $B^c \neq 0$, so

$$2\pi^2 \dot{N}_{CS} = E^c \cdot B^c + E^* \cdot B^* \tag{58}$$

would change value if for some reason one orthogonally departed from the constraint manifold.

This is the source of problems for the implementation of a chemical potential for N_{CS}, which modifies the E equation of motion by

$$\delta \dot{E} = -\mu \frac{\partial \dot{N}_{CS}}{\partial E} = \frac{-\mu}{2\pi^2} B\,. \tag{59}$$

Since $B^c \neq 0$ this moves E^c away from zero, which in turn changes the value of $\dot{N}_{CS}$, producing wrong answers. What has happened is that we have added a new term to the Hamiltonian, with a part linear in E^c, so the constraint is no longer first class. The evolution then departs from the constraint manifold. But if we redefine $\dot{N}_{CS}$ as

$$2\pi^2 \dot{N}_{CS} = E^* \cdot B^*\,, \tag{60}$$

which coincides with the previous definition on the constraint manifold, then the constraint will again be first class and the evolution will not violate Gauss' law. The modification to the E field equation of motion becomes

$$\delta \dot{E}^* = -\frac{\mu}{2\pi^2} B^* \,, \qquad \delta \dot{E}^c = 0 \,, \tag{61}$$

which preserves the Gauss constraints. And since we never leave the constraint surface, we can still compute $\dot{N}_{CS}$ using $E \cdot B$.

The easiest way to implement this addition to the equation of motion is to apply Eq. (59) but to then remove the contribution to E^c by orthogonally projecting to the constraint surface. An exact orthogonal projection is numerically expensive; a very accurate approximate algorithm, which is exactly orthogonal but does not quite complete the projection, was developed in [21] (which is where the interested reader should go for more thorough details). It is also shown there that this technique gives a value for Γ_μ equal to $\Gamma_d/2$, in accord with the fluctuation dissipation relation, a good check.

In the case of Yang-Mills Higgs theory, it is no longer true that $E^c = 0$; instead the Gauss constraints stipulate that

$$\forall x, a \qquad -\operatorname{Re}\left(\Pi^\dagger(x) i\tau^a \Phi(x)\right) + \sum_i \left[E_i^a(x) - (U_i^\dagger(x-i) E_i(x-i) U_i(x-i))^a\right] = 0 \,. \tag{62}$$

To analyze the application of a chemical potential it is convenient to consider an orthonormal basis for the momenta E, Π which partitions into 4 subcatagories: the E^*; the radial components of Π; an orthonormal basis of the linear combinations of degrees of freedom which are forced zero by the Gauss constraints, P^c; and an orthonormal basis of the remaining degrees of freedom, P^*. P^c and P^* are mixtures of the E^c and Higgs momentum degrees of freedom. The definition of $\dot{N}_{CS}$ can be written as

$$2\pi^2 \dot{N}_{CS} = B \cdot E = B^* \cdot E^* + B^c \cdot P^* + B^c \cdot P^c \,, \tag{63}$$

where the dot products involving the P are between B and the E field components of the P. As above, applying a chemical potential using this definition of $\dot{N}_{CS}$ will excite violations of the Gauss constraints; again the solution is to say that the definition of $\dot{N}_{CS}$ is

$$2\pi^2 \dot{N}_{CS} = B^* \cdot E^* + B^c \cdot P^* \,, \tag{64}$$

which is equivalent on the constraint manifold and therefore does not require a change in the program code which computes it. All that changes is that the momenta should be orthogonally projected to the constraint manifold each update. The algorithm for this orthogonal projection is the same as the algorithm proposed for use in thermalizing Yang-Mills Higgs theory in [21] and used in this paper for the canonical ensemble algorithm.

A.3 Results for N_{CS} motion in Yang-Mills Higgs theory

Now we will apply these tools to investigate the motion of N_{CS} in Yang-Mills Higgs theory in each phase. Data for the diffusion rate in Yang-Mills and Yang-Mills Higgs

Theory	β_L	m_{H0}	Phase	t	κ_d	"expected errorbar"
YM	6	N.A.	N.A.	1000	$1.05 \pm .11$	$\pm.18$
YMH	$\simeq 8$	-.3223	symmetric	4000	$0.85 \pm .07$	$\pm.14$
YMH	$\simeq 8$	-.3223	broken	8000	$0.111 \pm .009$	$\pm.037$
YMH	8	-.50	deep broken	3000	$0.059 \pm .008$	$\pm.04$

Table 2: Diffusion rates of N_{CS} in Yang-Mills and Yang-Mills Higgs theory. In the last column the bare Higgs mass squared was $m_{H0} = -0.5$ in lattice units, placing the system deep in the broken phase. The "expected errorbar" is the errorbar which would occur if the diffusion were made out of Poisson distributed integer steps.

theory are given in Table 2. As has become standard in the literature, the rate is expressed in terms of

$$\kappa_d \equiv \Gamma_d (\pi \beta_L)^4 \text{ lattice units} \quad \text{or} \quad \Gamma_d (\alpha_w T)^{-4} \text{ physical units}. \tag{65}$$

All data are for 16^3 lattices, which should be large enough to achieve the infinite volume limit for the values of β_L used [20]. The Yang-Mills Higgs data are all for (bare) $\lambda_L = 0.20$. To illustrate the data analysis technique, Figure 11 shows a 6000 lattice unit section of the evolution of the Yang-Mills Higgs system in the broken phase, and Figure 12 gives the coefficients of the sine transform, clearly showing the $A/n^2 + B$ behavior as well as the wide scatter associated with the log of the square of a Gaussian quantity.

There are three pieces of evidence which make it difficult to believe that the observed diffusion constant in the broken phase represents genuine infrared, topology changing physics. The first is rather subtle; it involves error bars. A series of integer steps in N_{CS} would not appear as perfect diffusive motion, and this would be reflected in the error bars in the extracted diffusion constant; if the steps were Poisson distributed, as seems reasonable, then N steps would give error bars in Γ_d of $\Gamma_d/\sqrt{N}$. The number of steps, based on Γ_d, is $\Gamma_d V t$, and the error estimate based on this reasoning is shown in the last column of the table. In the broken phase the actual error bars are much too small, suggesting that the diffusive process is somehow much smoother than expected. This would happen if it was the accumulation of a large set of small, ultraviolet shifts in N_{CS}.

Ambjorn and Krasnitz have shown that, at leading order, the ultraviolet theory behaves like an abelian theory, and shifts in N_{CS} are elastic, and are restored a moment later [20]. But they also show that such shifts occur at a rate which diverges as $a \to 0$, so if at next to leading order such shifts are not perfectly restored, it could still contribute an effect which would not vanish as $a \to 0$. This motivates the possibility of a spurious signal which remains constant in the small a limit, which would neatly explain the behavior of the diffusion rate observed above.

For a further piece of evidence, we applied a very large chemical potential, $\mu = 6/\beta_L$, to a 16^3 lattice of Yang-Mills Higgs plasma in the broken phase just below the phase transition temperature. Over a time period of $t = 4000$, N_{CS} changed by 11.4, which would correspond to $\kappa_d = .088 \pm .026$ if $\dot{N}_{CS}$ rises linearly with μ out to

$6/\beta_L$. Since this agrees with the measured value of κ_d, we conclude that the response is indeed linear. However, if there were a substantial free energy barrier we would expect the rate to rise with $\sinh(2\beta_L\mu)$, which it clearly does not. Since symmetry is broken strongly enough at the value of λ_L we are considering that there should be a substantial free energy barrier, this implies that the effect we observe is not the system jumping that barrier, but some other process, presumably the ultraviolet effect suggested above. This evidence is in the same spirit as the first piece.

For a final, strong piece of evidence, consider the last line in the table. Here we evolved a volume of Yang-Mills Higgs fluid with a large negative Higgs mass squared, so it was very deep in the broken phase; in fact we measured $\beta_L^2\Phi^\dagger\Phi = 98$, over 5 times its value in the broken phase just after the phase transition for the parameter values we have concentrated on in most of this paper. This corresponds, in physical units, and after subtracting off the ultraviolet $1/a$ contribution, to $\phi = 4.7gT$. The tree level Sphaleron energy for this value of ϕ is $4.7 \times 4\pi B(\lambda/g^2)T \simeq 100T$ [54]. For such a large value, the semiclassical Sphaleron approximation should be very reasonable, and the diffusion rate should have an immense exponential suppression, by a factor on order $\exp(-100)$ [54, 4]; yet the measured rate is only mildly lower than that barely inside the broken phase. This diffusion of N_{CS} *must* be a lattice artefact, unless our understanding of baryon number violation deep in the broken phase is completely wrong. The slight decline in the rate relative to the rate "just" inside the broken phase probably comes about because ϕ is larger even than the lattice inverse spacing, so even the ultraviolet lattice modes have their populations mildly suppressed.

We should point out that, while the error bars for diffusion in Yang-Mills theory and in the symmetric phase of Yang-Mills Higgs theory are also smaller than expected, they are not as much smaller, and the argument that N_{CS} should diffuse in integer steps is invalid in the unbroken phase. Further, it has been demonstrated that the diffusion rate falls off for small volumes, which shows that the dominant contribution is indeed infrared and should reflect real physics [20]. It is likely that a small part $\sim 10\%$ of the measured rate in the symmetric phase and in Yang-Mills theory arises from ultraviolet artefacts; in fact the results here could be viewed as a calibration of that contribution, since the ultraviolet behavior of lattice Yang-Mills Higgs theory should be about the same in each phase.

B Bubble wall surface tension

In this appendix we present the details of the calculation of the bubble wall surface tension. The determination has two parts: first we identify the bubble wall surfaces, then we show how to extract the surface tension from the shape of the surface (averaging over a large sample of surfaces). The reader can skip the first subsection and just take the wall surface position to be known if they are uninterested in numerical details.

B.1 Finding the surface

Suppose we have the values of Φ and the connections U at some point in time and we want to determine where the phase boundary is. The problem is that Φ contains a lot of ultraviolet fluctuations, so a simple threshold definition of the two phases does not work. We will need to coarse grain or smooth the fields. Define the once smoothed Higgs field Φ_1 as

$$\Phi_1(x) = \frac{1}{4}\Phi(x) + \frac{1}{8}\sum_i \left[U_i(x)\Phi(x+i) + U_i^\dagger(x-i)\Phi(x-i)\right]. \tag{66}$$

The sum just averages over nearest neighbors, parallel transporting along the shortest path. Φ_{n+1} is defined by applying the same averaging process to Φ_n. For large n, Φ_n is approximately Φ averaged over a Gaussian envelope of variance $3n/4$. The averaging very quickly removes ultraviolet fluctuations. It also very slowly degrades the condensate, because the averaging includes an averaging over different parallel transport paths, and the trace of any Wilson loop is less than TrI. After several smoothings (we use Φ_8, but for a finer lattice or a larger value of λ_L we would need to use more) the phases become much more distinct, although one still cannot distinguish them by setting a threshold.

To work with a real c number quantity we take $\Phi_n^\dagger\Phi_n$. Label the three directions x_1, x_2, and x_3, with x_3 the long direction in the lattice. For each column (fixed x_1 and x_2) we smooth along the column with a Gaussian envelope of width large enough to make the two phases distinguishable by a threshold, but smaller than the typical wall thickness (which for our value of λ_L and β_L will turn out to be on order 15). In practice we find a width $\simeq 7$ is sufficient. (If it is impossible to smooth enough that the two phases can always be distinguished by a threshold without making the smoothing length larger than the wall thickness, then one should have used more gauge invariant smoothings earlier.) Call the function we get by doing this smoothing $f(x_1, x_2, x_3)$. The only problem left is to choose a threshold by which to define the phases. We do this as follows. First, for each column we find the minimum and maximum values of f; average these over the columns; call them f_{min} and f_{max}. We assume that any point with f more than halfway from f_{min} to f_{max} is in the broken phase and any point less than 0.2 of the way is in the symmetric phase, and from this definition we find the average value of f in each phase. Then we set a threshold some percentage of the way between the average symmetric phase value of f and the average broken phase value of f; at equilibrium the choice is 30%, reflecting that fluctuations in f are much larger in the broken phase; but for a heavily supercooled system we set the threshold higher, 40%, because the symmetric phase fluctuations become larger.

With the threshold set, we define the wall height function $z(x_1, x_2)$ by starting at the value of x_3 in the x_1, x_2 column where f is minimum and incrementing x_3 until the first point is reached where the threshold is exceeded; $z(x_1, x_2)$ is chosen as the value of x_3 where this happens. The other surface is found by moving backward.

The definition of the surface described here is imperfect; it assumes that the surface is single valued (never bending more than 90° from horizontal) and it smooths the surface at a length scale on order the Gaussian envelope radius used to define the

smoothed Higgs field Φ_n. However, the surface is not really well defined on length scales much shorter than the wall thickness, and we will be most interested in infrared scales on which the surface should look relatively flat, so neither problem will be of consequence.

B.2 Determining the surface tension

Take the height function $z(x_1, x_2)$ to be known; how can one determine the surface tension from it?

The free energy of a surface with surface tension σ and height function z is the area of the surface times the surface tension,

$$F = \sigma \int d^2x \sqrt{1 + (\nabla z)^2}\,. \tag{67}$$

At finite temperature, surface waves will be excited and the partition function for the appearance of the surface will be

$$Z = \int \mathcal{D}z \exp(-\beta F)\,, \tag{68}$$

which is the partition function of a simple two dimensional Euclidean field theory. In the infrared we can expand F as

$$F = \sigma \int d^2x \left(1 + \frac{1}{2}(\nabla z)^2 - \frac{1}{8}((\nabla z)^2)^2 + \ldots\right)\,. \tag{69}$$

The first term contributes a z independent constant and the remaining terms describe a free massless field theory plus nonrenormalizeable operators. These operators will cause some renormalization of σ between an ultraviolet scale and the deep infrared, but because they are nonrenormalizeable σ will have an unambiguous deep infrared limit, which is the value of interest in any calculation where the surface tension is a useful concept. concentrating on the infrared and remembering that there may be corrections for ultraviolet modes, and taking the area over which the surface is stretched to be an $L \times L$ square,

$$\beta F \simeq \frac{\sigma}{T} \int_0^L \int_0^L d^2x \left(1 + \frac{1}{2}(\nabla z)^2\right)\,. \tag{70}$$

This free field theory is trivially solved by Fourier transformation. Defining

$$\tilde{z}_{\vec{n}} = \int \frac{d^2x}{L^2} z(x) e^{2\pi i \vec{n}\cdot x/L} \tag{71}$$

we find

$$\beta F = \sum_{\vec{n}} \frac{4\pi^2 \sigma n^2 \tilde{z}_n^2}{2T} \tag{72}$$

and by equipartition

$$\langle \tilde{z}_n^2 \rangle = \frac{T}{4\pi^2 \sigma n^2}\,. \tag{73}$$

This expression should be obeyed in the limit of large L/n; for smaller values of L/n it will have corrections because of the nonrenormalizeable operators, and in the numerical calculation it will have corrections in the ultraviolet because of the properties of the numerically determined bubble wall surface mentioned earlier. To compute the surface tension it will then be necessary not only to average the $\tilde{z}_n$ over a large sample of walls, but to perform an extrapolation to zero n. Because the corrections to the free field theory are nonrenormalizeable, the corrections to Eq. (73) will appear as powers of $(n/L)^2$; there will be no logarithmic corrections. As discussed in the text we performed the large L/n extrapolation by fitting $n^2\langle\tilde{z}_n^2\rangle$ to $A\exp(-Bn^2)$. We do not know of a good physical motivation for this form except that it resembles what a Gaussian smoothing of the wall surface would do to the $\tilde{z}_n$. In practice we could equally well fit only the first few points to a straight line; the result is about the same.

References

[1] A. Sakharov, JETP Lett. **6** (1967) 24.

[2] G. t'Hooft, Phys. Rev. Lett. **37** (1976) 8.

[3] V. Kuzmin, V. Rubakov, and M. Shaposhnikov, Phys. Lett. **D 30** (1985) 36.

[4] P. Arnold and L. McLerran, Phys. Rev. **D 36** (1987) 581.

[5] N. Turok and J. Zadrozny, Phys. Rev. Lett. **65** (1990) 2331; Nucl. Phys. **B 358** (1991) 471.

[6] L. McLerran, M. Shaposhnikov, N. Turok, and M. Voloshin, Phys. Lett. **B 256** (1991) 451.

[7] A. Nelson, D. Kaplan, and A. Cohen, Nucl. Phys. **B 373** (1992) 453.

[8] M. Dine, P. Huet, R. Singleton and L. Susskind, Phys. Lett. **B257**, 351 (1991).

[9] K. Kajantie, M. Laine, K. Rummukainen, and M. Shaposhnikov, Nucl. Phys. **B 458** (1996) 90.

[10] J. Cline and K. Kainulainen, CERN-TH/96-76, hep-ph/9605235; M. Losada, RU-96-25, hep-ph/9605266; M. Laine, Nucl. Phys. **B 481**, 43 (1996).

[11] L. Dolan and R. Jackiw, Phys. Rev. **D 9** (1974) 3320.

[12] P. Arnold and O. Espinosa, Phys. Rev. **D 47** (1993) 3546; Phys. Rev. **D 50** (1994) 6662.

[13] Z. Fodor and A. Hebecker, Nucl. Phys. **B 432** (1994) 127.

[14] K. Farakos, K. Kajantie, K. Rummukainen, and M. Shaposhnikov, Nucl. Phys. **B 425** (1994) 67.

[15] K. Farakos, K. Kajantie, K. Rummukainen, and M. Shaposhnikov, Nucl. Phys. **B 442** (1995) 317.

[16] K. Kajantie, M. Laine, K. Rummukainen, and M. Shaposhnikov, Nucl. Phys. **B 466** (1996) 189.

[17] D. Grigorev and V. Rubakov, Nucl. Phys. **B 299** (1988) 248.

[18] J. Ambjorn, M. Laursen, and M. Shaposhnikov, Nucl. Phys. **B 316** (1989) , 483.

[19] J. Ambjorn, T. Askgaard, H. Porter, and M. Shaposhnikov, Nucl. Phys. **B 353** (1991) 346.

[20] J. Ambjorn and A. Krasnitz, Phys. Lett. **B 362** (1995) 97.

[21] G. D. Moore, Nucl. Phys. **B 480** (1996) 657.

[22] G. D. Moore, Nucl. Phys. **B 480** (1996) 689.

[23] W. Tang and J. Smit, Nucl. Phys. **B 482** (1996) 265.

[24] K. Kajantie, K. Rummukainen, and M. Shaposhnikov, Nucl. Phys. **B 407** (1993) 356; K. Farakos, K. Kajantie, K. Rummukainen, and M. Shaposhnikov, Nucl. Phys. **B 425** (1994) 67; Phys. Lett. **B 336** (1994) 494.

[25] N. Landsman, Nucl. Phys. **B 332** (1989) 498.

[26] D. Bodeker, AD-THEP-96-27, hep-th/9609170.

[27] T.S. Evans and D.A. Steer, Nucl. Phys. **B 474** (1996) 481.

[28] E. Braaten and R. Pisarski, Nucl. Phys. **B 337** (1990) 569.

[29] D. Bodeker, L. McLerran, and A. Smilga, Phys. Rev. **D 52** (1995) 4675.

[30] E. Braaten and R. Pisarski, Phys. Rev. **D 42** (1990) 2156; Phys. Rev. **D 46** (1992) 1829.

[31] J. Kogut and L. Susskind, Phys. Rev. **D 11** (1975) 395.

[32] F. Csikor, Z. Fodor, J. Hein, and J. Heitger, Phys. Lett. **B 357** (1995) 156; F. Csikor, Z. Fodor, J. Hein, A. Jaster, and I. Montvay, Nucl. Phys. **B 474** (1996) 421; M. Guertler, E. Ilgenfritz, J. Kripfganz, H. Perlt, and A. Schiller, hep-lat/9512022; hep-lat/9605042.

[33] J. Kripfganz, A. Laser, and M. Schmidt, HD-THEP-95-53, hep-ph/9512340.

[34] N. Turok, Phys. Rev. Lett. **68** (1992) 1803.

[35] K. Enqvist, J. Ignatius, K. Kajantie, and K. Rummukainen, Phys. Rev. **D 45** (1992) 34415; J. Ignatius, K. Kajantie, H. Kurki-Suonio and M. Laine, Phys. Rev. **D 49** (1994) 3854.

[36] M. Dine, R. Leigh, P. Huet, A. Linde, and D. Linde, Phys. Rev. **D 46** (1992) 550.

[37] B. Liu, L. McLerran, and N. Turok, Phys. Rev. **D 46** (1992) 2668.

[38] S. Khlebnikov, Phys. Rev. **D 46** (1992) 3226.

[39] P. Arnold, Phys. Rev. **D 48** (1993) 1539.

[40] A. Heckler, Phys. Rev. **D 51** (1995) 405.

[41] G. Moore and T. Prokopec, Phys. Rev. Lett. **75** (1995) 777.

[42] G. Moore and T. Prokopec, Phys. Rev. **D 52** (1995) 7182.

[43] H. Kurki-Suonio and M. Laine, Phys. Rev. **D 54** (1996) 7163.

[44] S. Jeon, Phys. Rev. **D 52** (1995) 3591.

[45] A. Krasnitz, Nucl. Phys. **B 455** (1995) 320.

[46] A. Krasnitz, private communication.

[47] N. Turok, in "Perspectives on Higgs Physics", Ed. G. Kane, World Scientific, 1993.

[48] D. Grigoriev, M. Shaposhnikov and N. Turok, Phys. Lett **275B** (1992) 395.

[49] M. Dine and S. Thomas, Phys. Lett. **B 328** (1994) 73.

[50] M. Joyce, T. Prokopec and N. Turok, Physical Review **D53**, 2930 (1996); Physical Review **D53**, 2958 (1996); Physical Review Letters **75**, 1695 (1995).

[51] See e.g. M. Dine, Nucl.Phys.Proc.Suppl. **37A**, 127 (1994).

[52] S. Khlebnikov and M. Shaposhnikov, Nucl. Phys. **B308** (1988) 885.

[53] V. Rubakov and M. Shaposhnikov, CERN-TH-96-13, hep-ph/9603208.

[54] F. Klinkhamer and N. Manton, Phys. Rev. **D 30** (1984) 2212.

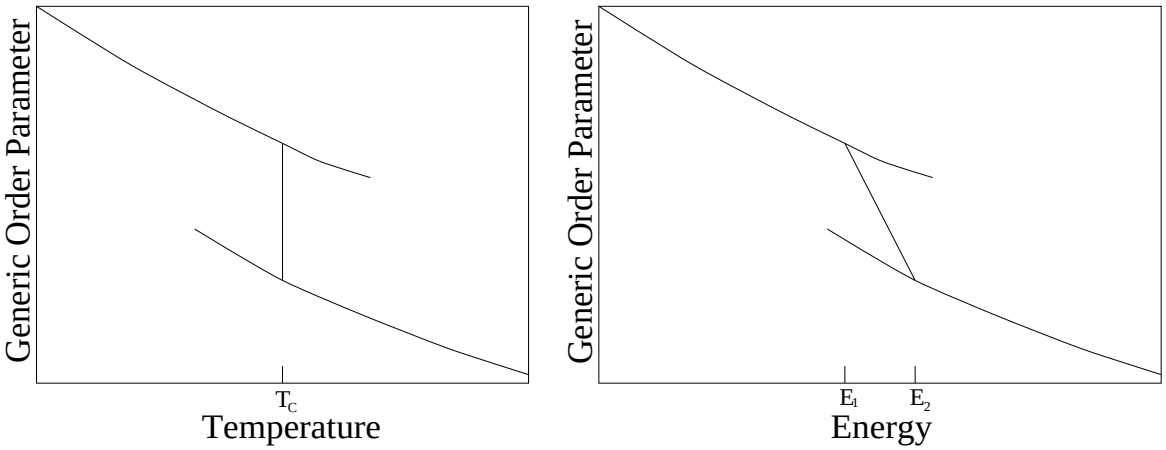


Figure 1: Schematic depiction of the dependence of an order parameter on temperature and energy, including metastability lines and the equilibrium coexistence line. Though equilibrium phase coexistence only occurs precisely at T_c, it happens for a range of energies between E_1 and E_2. Phase mixture is stable for a fixed energy system if the energy is in this range.

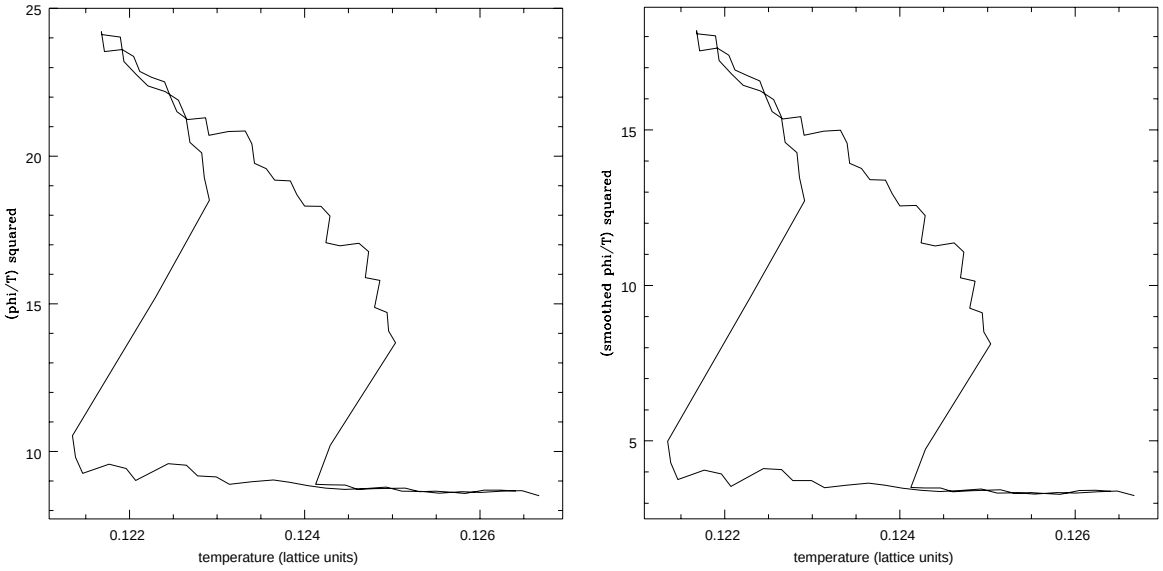


Figure 2: Lattice $\Phi^\dagger\Phi/T^2$ as a function of temperature $(1/\beta_L)$ for a 30^3 lattice; at left, without smoothing, and at right, with one nearest neighbor smoothing. The system begins in the symmetric phase at high temperature and is cooled through the phase transition, and is then heated back to the original temperature. The system supercools during the cooling and superheats during the heating, resulting in a hysteresis loop. The cooling represents a total elapsed time of 1280 lattice units; the heating is twice as long, with longer bins, to suppress fluctuations. The fluctuations in $\Phi^\dagger\Phi/T^2$ are much larger in the broken than the symmetric phase, except near where the symmetric phase becomes unstable, where the fluctuations become larger. Both the jump in the order parameter and the fluctuations are almost identical before and after smoothing, so both are infrared phenomena; but the symmetric phase value of $\Phi^\dagger\Phi$ is primarily ultraviolet, and is suppressed by the smoothing.

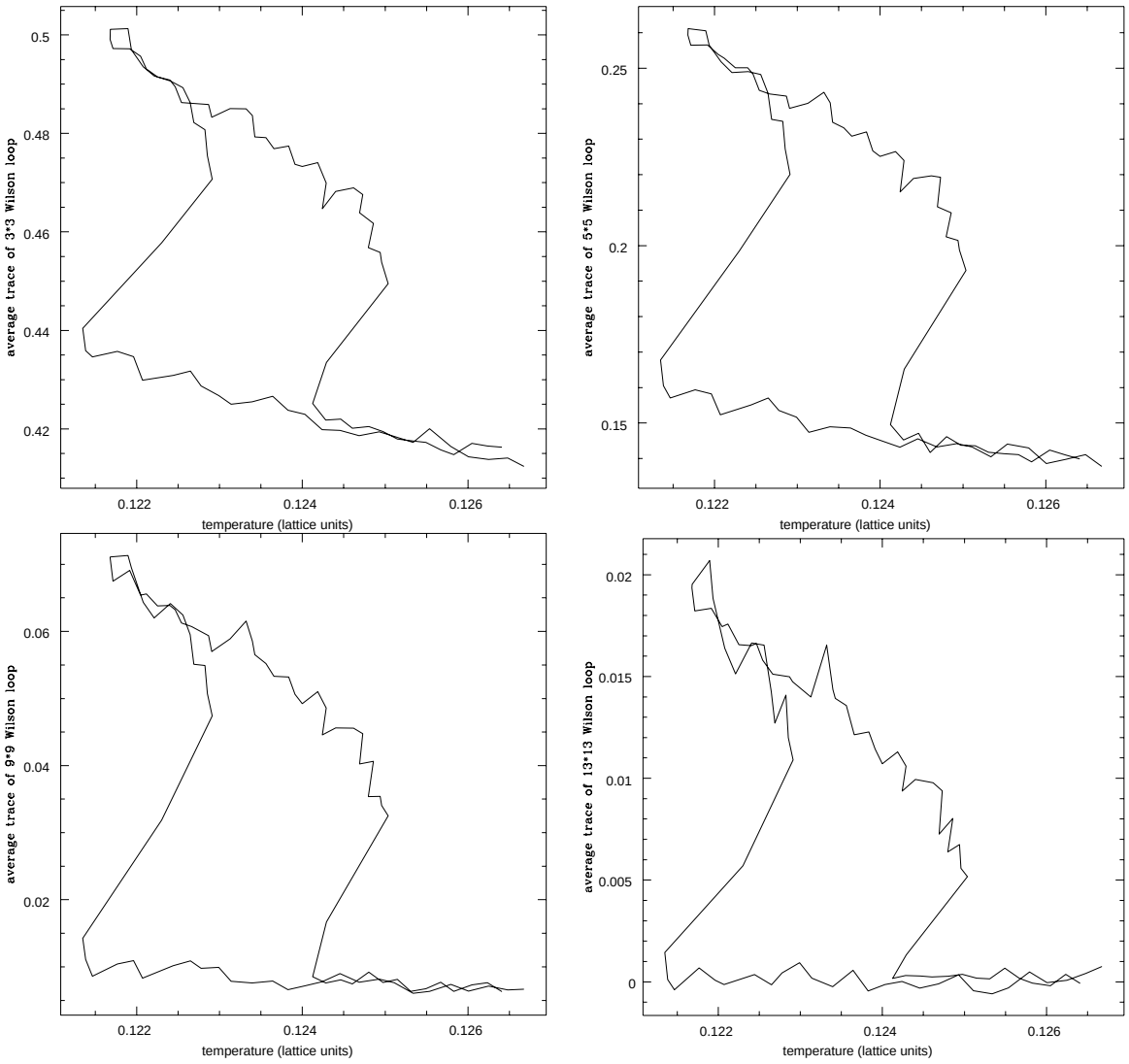


Figure 3: Average of the trace of some Wilson loops for the same run. The normalization is such that the trace is 1 in vacuum. Fluctuations in the Wilson loops are about the same size in each phase, and they follow quite closely the fluctuations of $\Phi^\dagger\Phi$. For the 9×9 loop the symmetric phase Wilson loops are almost zero, showing no long range order; they are zero within tight statatistical error for 13×13 loops, and here the broken phase values are nearly zero as well.

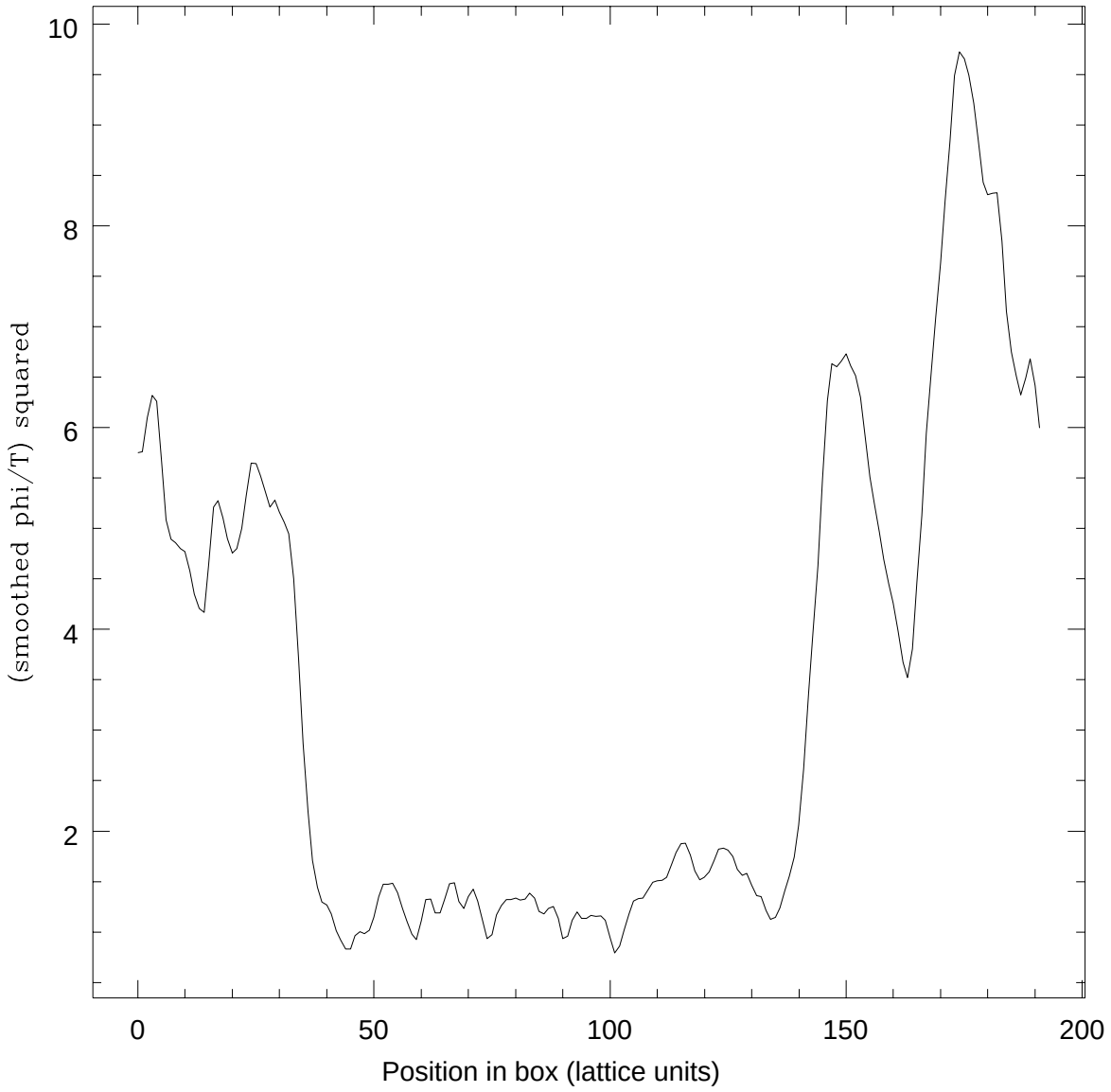


Figure 4: Six times smoothed Higgs field, averaged over the short directions of a $16 \times 16 \times 192$ lattice at the equilibrium temperature $T \simeq 0.1241$, plotted as a function of position in the box. The two phases and the phase boundaries are clear, although the broken phase has quite sizeable fluctuations in the order parameter.

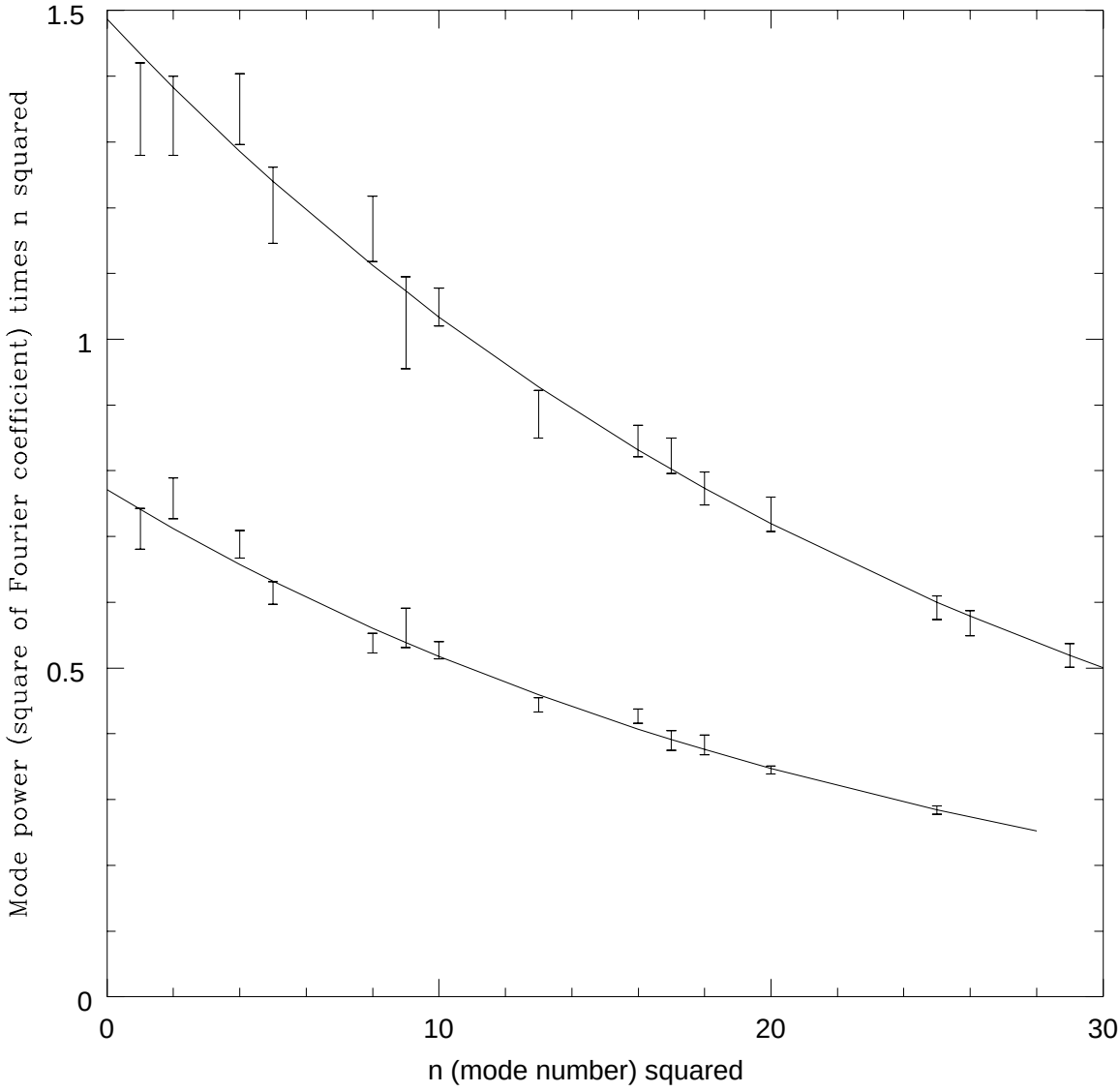


Figure 5: Bubble wall surface power spectrum: $\langle \tilde{z}_n^2 n^2 \rangle$ plotted against n^2. The upper data are for a 32×32 cross section box at $\beta_L = 8$ and the lower data are for a 36×36 cross section box at $\beta_L = 6$. The fit functions are exponentials, used to extrapolate the data to the infrared ($n = 0$) limit.

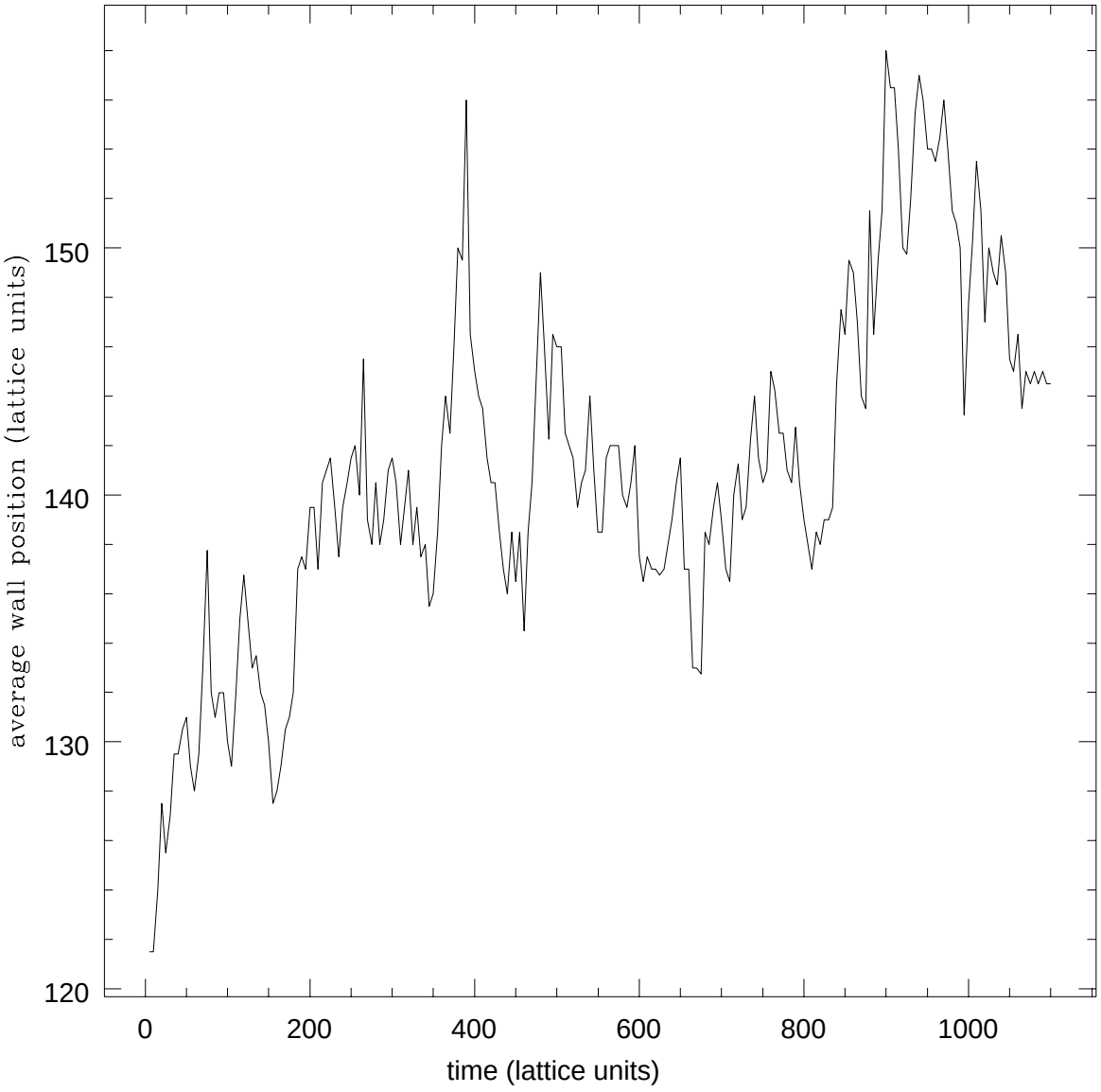


Figure 6: Average of positions of bubble walls as a function of time for a $16 \times 16 \times 192$ box at equilibrium with $\beta_L \simeq 8$. The motion should be Brownian.

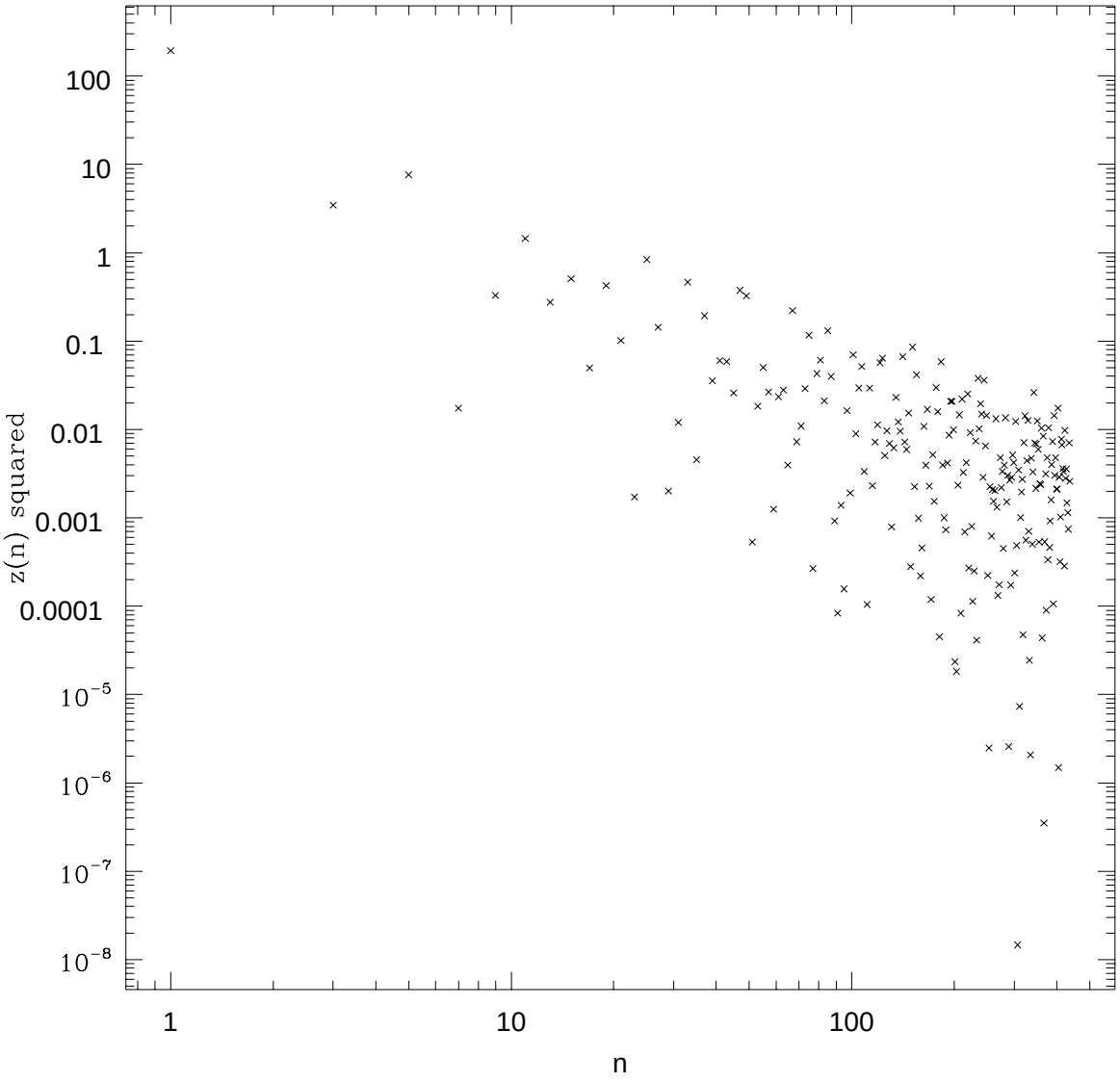


Figure 7: Power spectrum for the previous plot, obtained by sine transformation. The wide scatter is expected for the log of the square of a Gaussian distributed quantity. If the motion is Brownian then the points should be uncorrelated and should depend on n as $1/n^2$.

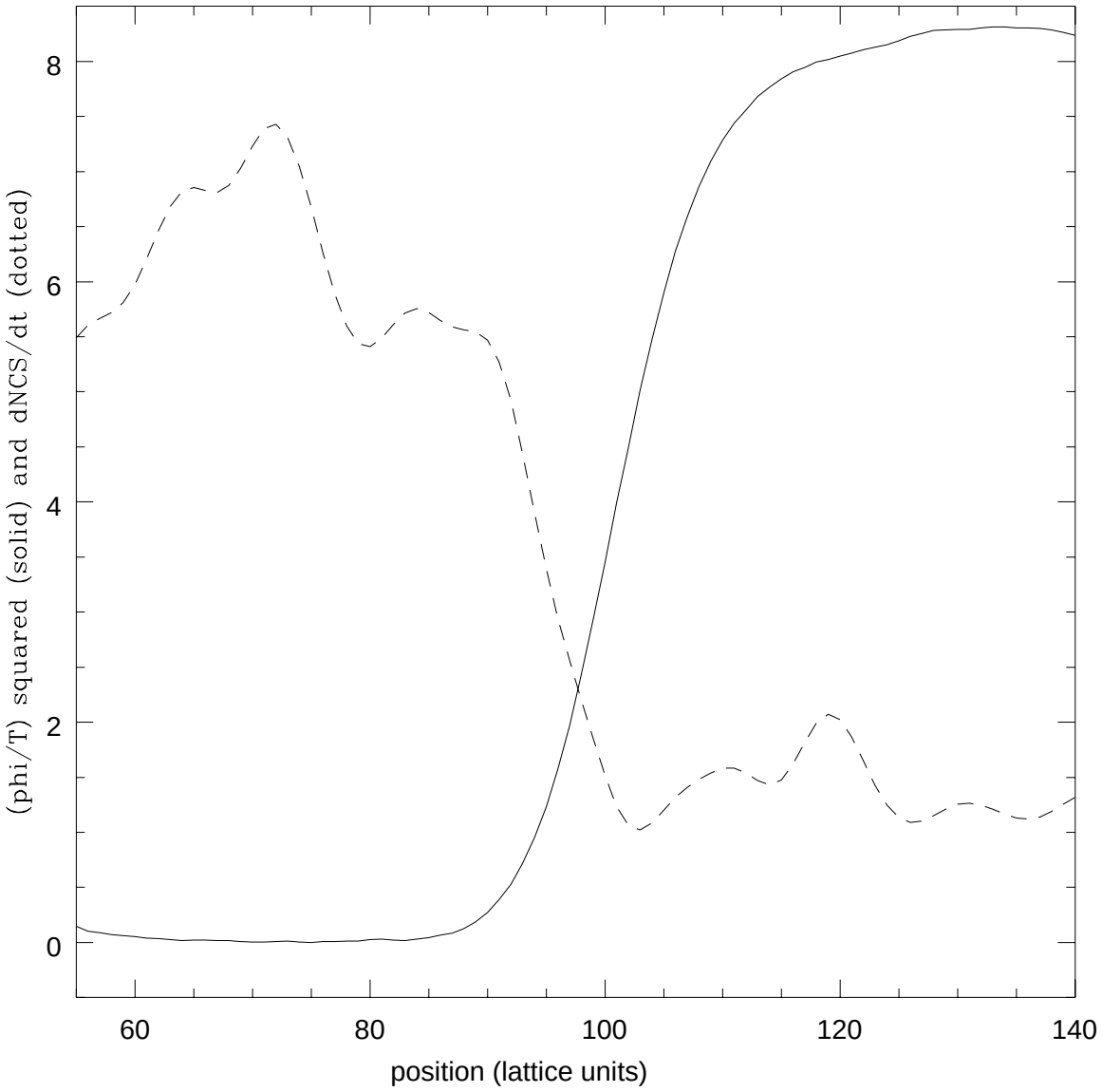


Figure 8: Wall shape in equilibrium (solid line). The vertical axis is $\Phi^\dagger\Phi\beta_L^2$ in lattice units, equal to $4(\phi^2/g^2T^2)$ in the continuum. The symmetric phase value has been subtracted. The horizontal axis is in lattice units, which equal $4/(\beta_L g^2 T) \simeq 1.2/T$ in physical units; the zeropoint of the axis is arbitrary. The dashed line shows dN_{CS}/dt in reponse to a constant chemical potential, as a function of position relative to this wall. The vertical scale for $\dot{N}_{CS}$ is arbitrary. The rate falls off sharply inside the wall.

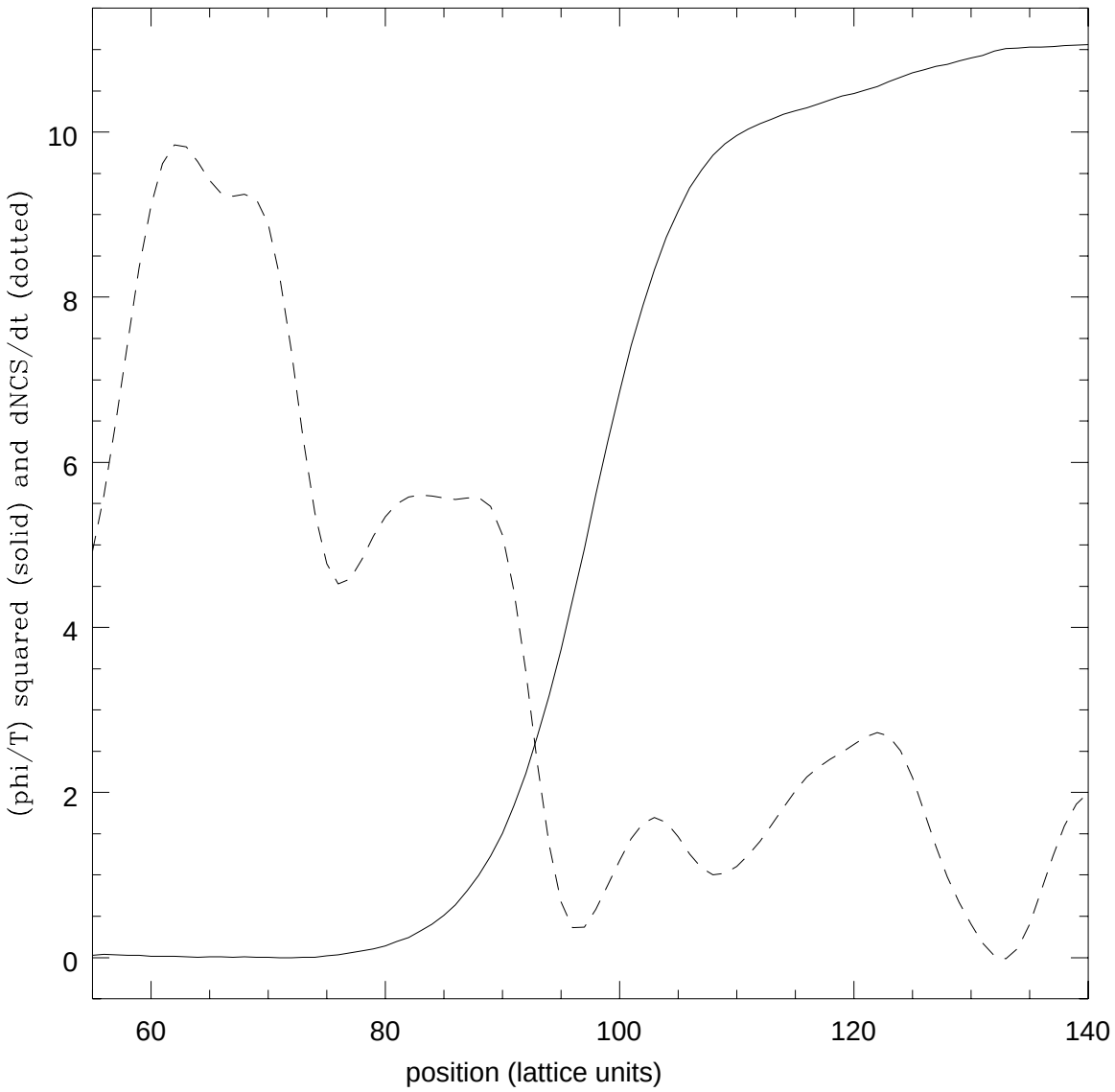


Figure 9: Wall shape out of equilibrium, below the phase transition temperature (solid line). The wall is in this case moving with a speed of $v \sim 0.3$. The dashed line shows dN_{CS}/dt in reponse to a constant chemical potential, as a function of position relative to this wall. Again the rate falls off sharply inside the wall. Axes as in previous Figure.

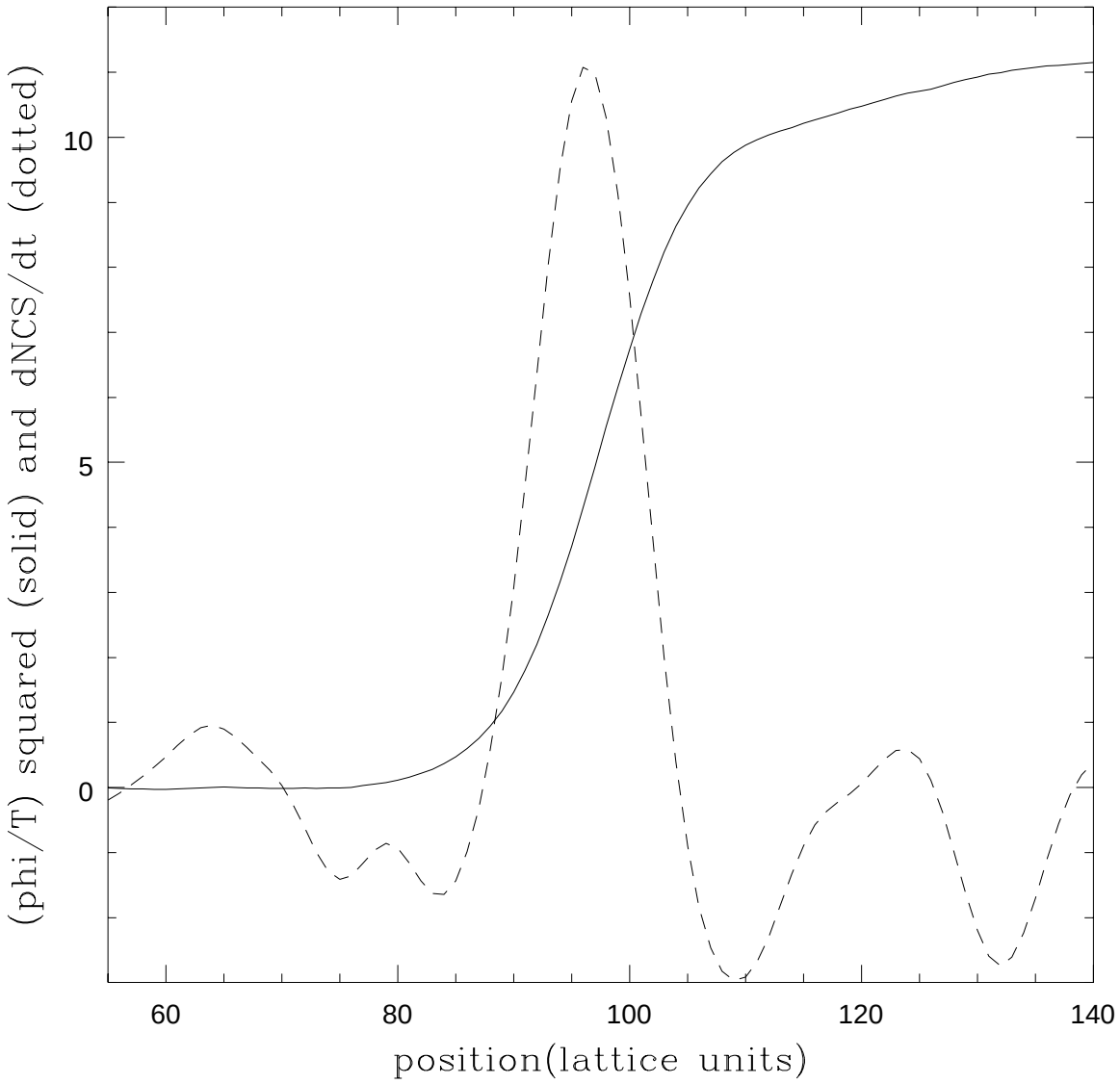


Figure 10: Bubble wall shape and $\dot{N}_{CS}$ when the chemical potential for N_{CS} was proportional to the gradient of the wall. The vertical axis for $\dot{N}_{CS}$ is arbitrary. There is a spike in $\dot{N}_{CS}$ on the wall, where the chemical potential was applied, and a pit on either side of the spike.

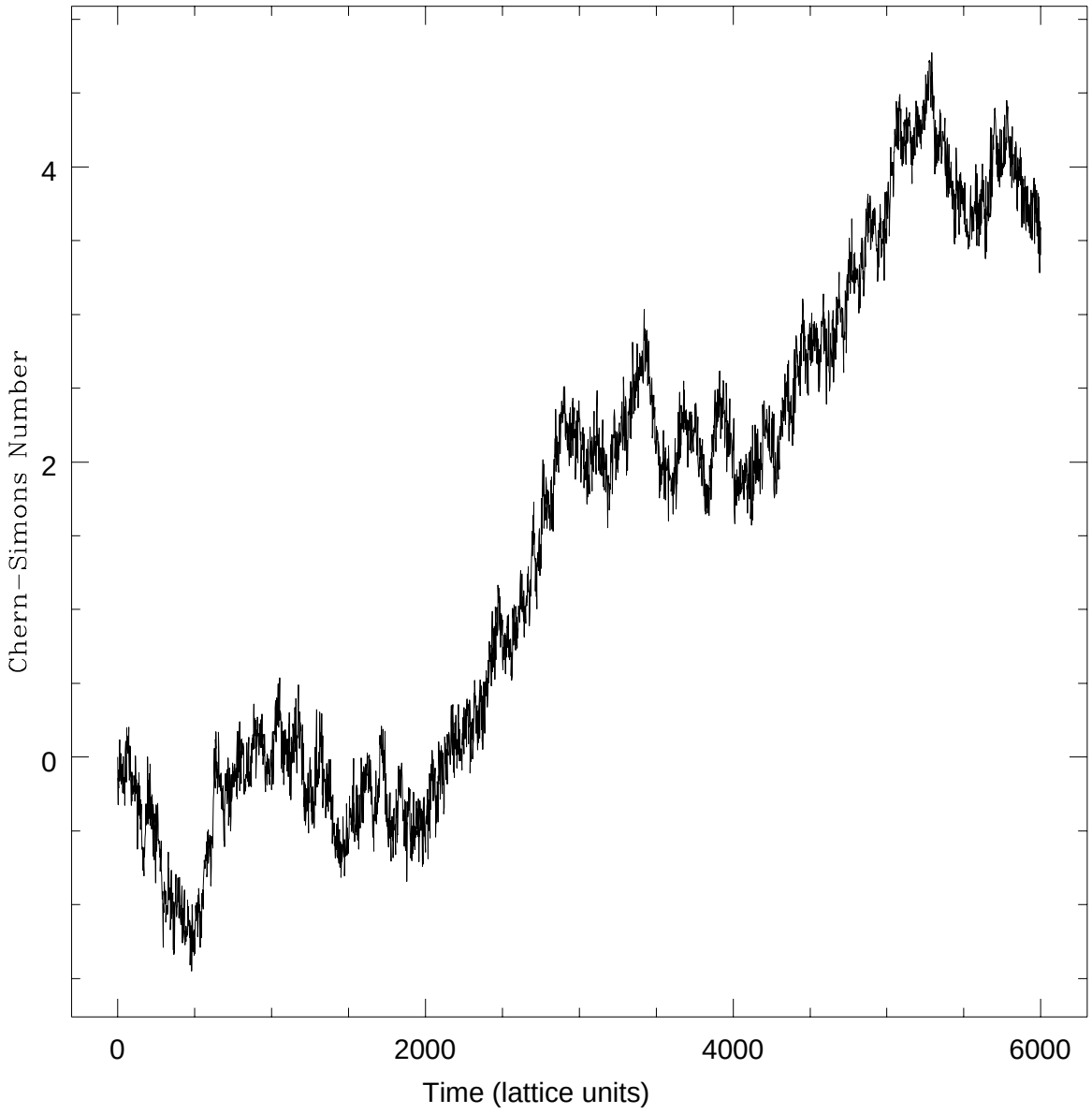


Figure 11: Chern-Simons number diffusing in the broken electroweak phase in a 16^3 box at $\beta_L \simeq 8$. The diffusion does not resemble sudden discrete jumps between integer spaced plateaus.

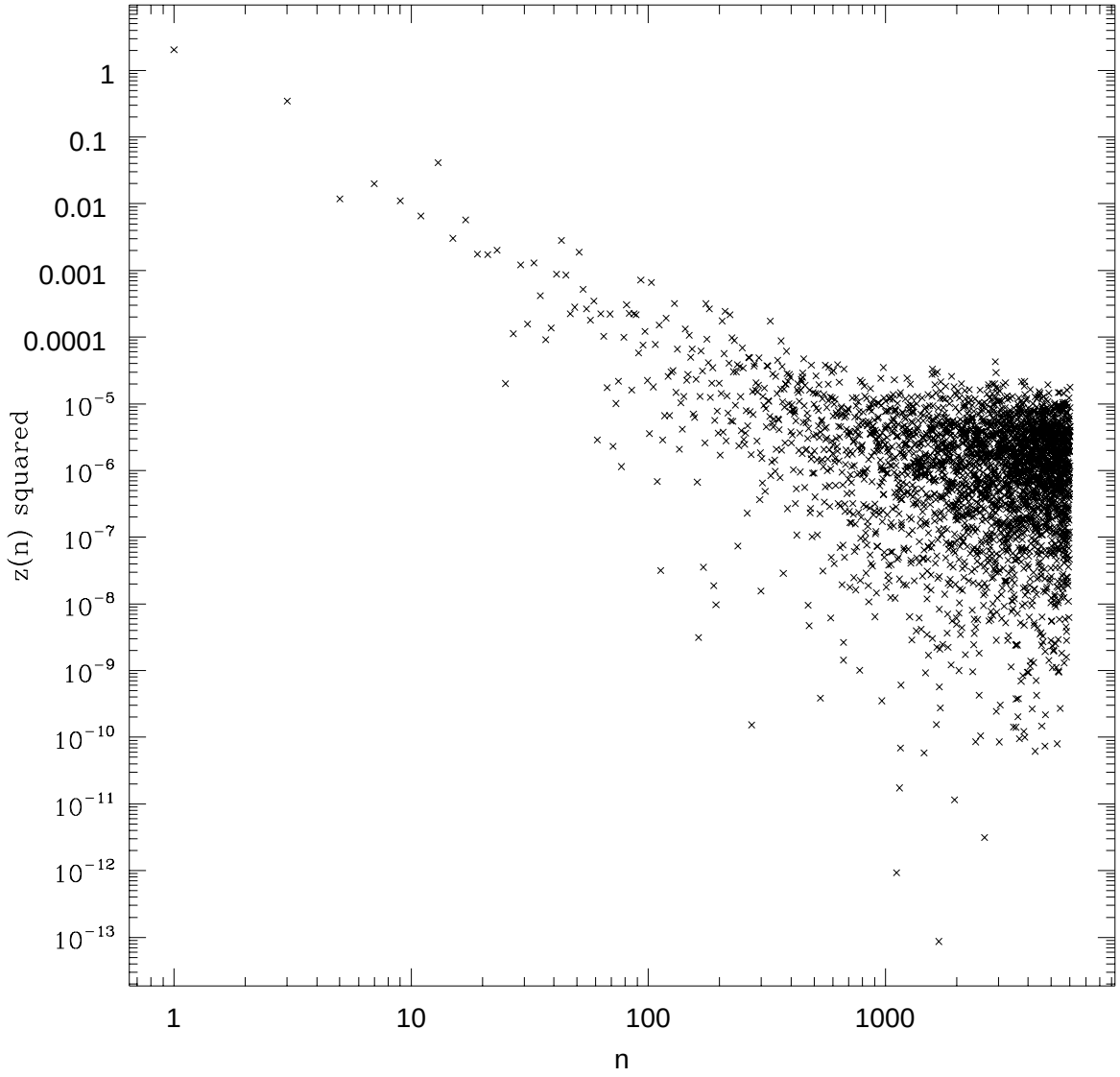


Figure 12: Sine transform of the previous data. The spectrum is in excellent agreement with white noise (constant power) plus a Brownian signal (power $\propto n^{-2}$). As discussed in the text, the Brownian motion is probably a lattice artefact.